CHARACTERIZATION OF A PUTATIVE TREHALOSE BIOSYNTHETIC PATHWAY IN SALMONELLA TYPHIMURIUM

A thesis presented to the faculty of the Graduate School of Western Carolina University in partial fulfillment of the requirements for the degree of Master of Science in Biology.

By

Connor Joseph Larmore

Director: Dr. Amanda Storm
Assistant Professor of Biology
Department of Biology

Committee Members: Dr. Scott Huffman, Chemistry
Dr. Heather Coan, Biology
Dr. Jamie Wallen, Chemistry

June 2023

TABLE OF CONTENTS

LIST OF TABLES

LIST OF FIGURES

ABSTRACT

CHARACTERIZATION OF A PUTATIVE TREHALOSE BIOSYNTHETIC PATHWAY IN SALMONELLA TYPHIMURIUM

Connor Joseph Larmore, M.S.

Western Carolina University (June 2023)

Director: Dr. Amanda Storm

Trehalose is a non-reducing disaccharide composed of two glucose monomers. In living organisms, this sugar is connected by an α-1,1-glycosidic linkage. In bacteria, trehalose is a component of various glycolipids and has been shown to confer abiotic stress tolerance. Genes believed to encode a trehalose biosynthetic pathway, including the enzymes maltooligosyl trehalose synthase (StMTSase) and maltooligosyl trehalose trehalohydrolase (StMTHase), have been identified in *Salmonella typhimurium* and shown by gene knockout to be essential for bacterial growth. However, the structure and activity of these types of enzymes have never been studied in any species of Proteobacteria. This study aimed to characterize the putative StMTSase and StMTHase enzymes. Comparative sequence and structure analysis revealed that both enzymes retain all the amino acids required for catalysis and are similar in overall architecture to functional homologs. Both enzymes also contain largely conserved substrate binding sites, although a tyrosine cluster identified in most other characterized MTSases is only partially conserved in the StMTSase. The putative StMTSase was biochemically characterized using the Nelson-Somogyi (NS) method for detecting reducing sugars, as MTSase enzymes convert reducing maltooligosaccharides into the non-reducing saccharide maltooligosyl trehalose. This enzyme was active on maltohexaose and dextrin but not maltotriose. It displayed the greatest

activity at 40°C, a pH of 7.0, and in a citrate phosphate (McIlvaine) buffer containing potassium. Finally, two mutant StMTSases were produced using site-directed mutagenesis. One mutant contained substitutions of tyrosine at two positions (M460Y and V464Y) to match residues forming part of the tyrosine cluster that is conserved in most other characterized MTSases. This enzyme displayed no detectable activity. The other mutant contained a single substitution of tyrosine (M460Y) and displayed activity comparable to the wild-type enzyme. Overall, this study provides evidence that the putative MTSase/MTHase trehalose biosynthetic pathway identified in *S. typhimurium* is functional. This study contributes to a better understanding of two reportedly essential *Salmonella* genes and their products, which could potentially be developed into therapeutic targets.

CHAPTER ONE: INTRODUCTION

Trehalose

Trehalose is a nonreducing disaccharide made of two glucose monomers. Several forms of this sugar exist, each differing in terms of the glycosidic linkage. These include α,β-1,1-trehalose, β,β-1,1-trehalose, and α,α-1,1-trehalose, with the last-mentioned being the form in living organisms.[1] Trehalose has been identified in many organisms, including bacteria, archaea, fungi, insects, plants, and algae. Within these, trehalose is multifunctional. This sugar is known to serve as a carbon and energy source, protect proteins and cell membranes when cells experience abiotic stress, and scavenge reactive oxygen species (ROS) to prevent cells from experiencing oxidative damage.[2]

Additionally, trehalose is a component of several bacterial glycolipids. The best studied is trehalose-dimycolate (cord factor) from *Mycobacterium tuberculosis*. This glycolipid reduces the permeability of the *M. tuberculosis* cell wall, conferring drug resistance.[1,2] Other trehalose-containing glycolipids, including 6,6,-diphosphatidyltrehalose (diPT) and 6-phosphatidyltrehalose (PT) in *Escherichia* and *Salmonella* isolates, have been identified. However, their potential roles in disease have yet to be elucidated.[1]

Trehalose Biosynthesis

Organisms can synthesize trehalose using a variety of biosynthetic pathways. The most common and best-studied of these is the TPS/TPP pathway. This pathway includes the enzymes trehalose-6-phosphate synthase (TPS) and trehalose-6-phosphate phosphatase (TPP). First, TPS catalyzes the transfer of a glucose moiety from a glucose sugar nucleotide, such as UDP-glucose or GDP-glucose, to glucose-6-phosphate. This results in trehalose-6-phosphate, which TPP

dephosphorylates to produce trehalose. This pathway has been identified in yeast, insects, bacteria, and the slime mold *Dictyostelium discoideum*.[2,3]

Additionally, trehalose can be synthesized by several pathways involving a single enzyme. First, the TreS pathway includes the enzyme trehalose synthase (TreS), which catalyzes the intramolecular rearrangement of maltose to trehalose.[2] Second, the TreP pathway consists of a trehalose phosphorylase enzyme (TreP), which generates trehalose from glucose-1-phosphate and glucose. Third, the TreT pathway includes a trehalose glycosyltransferring synthase enzyme (TreT), which forms trehalose from ADP-glucose and glucose. All of these pathways have been identified in bacteria.[1]

Finally, and most relevant to this project, trehalose can be synthesized by a pathway involving the enzymes maltooligosyl trehalose synthase (MTSase) and maltooligosyl trehalose trehalohydrolase (MTHase). This pathway is illustrated in Fig. 1, along with a description of sub-site nomenclature. In the first step, MTSase catalyzes an intramolecular transglycosylation reaction to convert the α-1,4-glycosidic linkage at the reducing end (contains a hemiacetal group) of maltooligosaccharides to an α-1,1-glycosidic linkage. This produces the saccharide maltooligosyl trehalose. Subsequently, MTHase hydrolyzes maltooligosyl trehalose, releasing trehalose and a shorter maltooligosaccharide.[4]

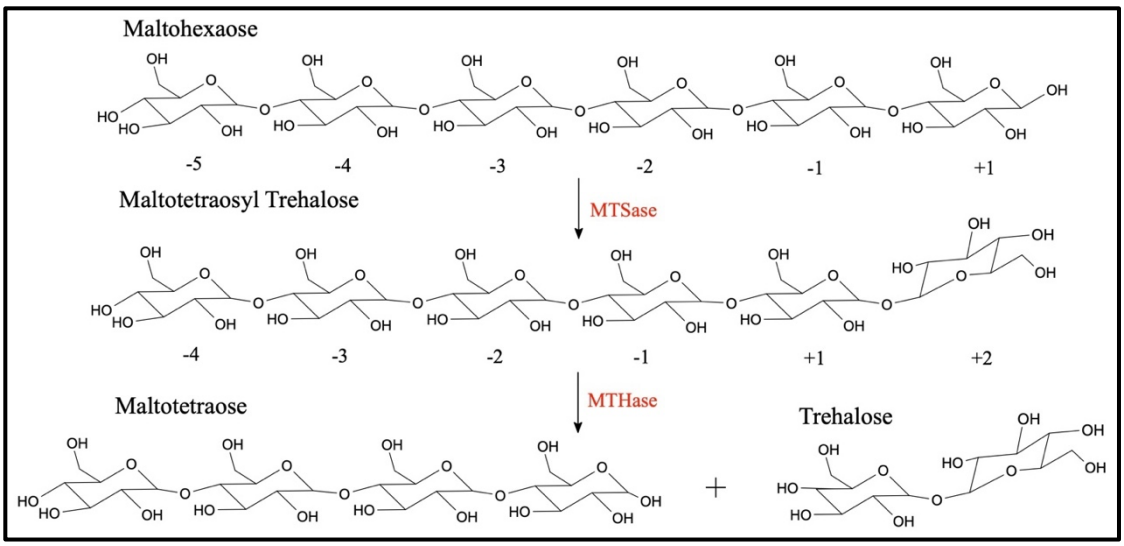

Fig. 1. The MTSase/MTHase trehalose biosynthetic pathway and sub-site nomenclature**.** Maltooligosyl trehalose synthase (MTSase) catalyzes an intramolecular transglycosylation reaction to convert the α-1,4-glycosidic linkage at the reducing end (contains a hemiacetal group) of maltooligosaccharides to an α-1,1-glycosidic linkage. Subsequently, maltooligosyl trehalose trehalohydrolase (MTHase) catalyzes the hydrolysis of maltooligosyl trehalose into trehalose and a shortened maltooligosaccharide. Maltohexaose and maltotetraosyl trehalose are labeled according to sub-site nomenclature. Sub-sites are labeled with increasingly negative numbers moving away from the cleavage point and towards the non-reducing end. Sub-sites are labeled with increasingly positive numbers moving away from the cleavage point and towards the reducing end.[5] This illustration was produced using MoleculeSketch.

This pathway has been chiefly studied in archaeal extremophiles of the genus *Sulfolobus*. These include *Sulfolobus acidocaldarius*, *Sulfolobus solfataricus* KM1, *Sulfolobus tokodaii*, and *Sulfolobus shibatae* DSM5389.[4,6–11] This is because thermostable MTSases and MTHases can be used for the industrial production of trehalose, a common sweetener, stabilizer of frozen and dried foods, and cosmetics additive.[4,12] Additionally, this pathway has been studied in the soil-dwelling bacterial species *Arthrobacter* sp. Q36 and the bacterial extremophile *Deinococcus radiodurans*.[13–15] However, this pathway has never been characterized for any species in the phylum Proteobacteria, which contains many pathogenic genera, including *Escherichia* and *Salmonella*.

Maltooligosyl Trehalose Synthase

Maltooligosyl trehalose synthases (MTSases) are classified into the glycoside hydrolase family 13 (GH13), the largest family of glycoside hydrolases. GH13 includes enzymes that act on substrates containing α-glycosidic bonds. Enzymes in this family are diverse, with some hydrolyzing α-glycosidic bonds and others catalyzing their formation via transglycosylation (transferring a sugar moiety from one glycoside to another).[16]

In 1995, Nakada et al. published the first characterization of an MTSase. This enzyme was identified in *Arthrobacter* sp. Q36, a Gram-positive bacterial species commonly found in soil. This enzyme catalyzes the intramolecular transglycosylation reaction previously mentioned and is active on maltooligosaccharides, including maltotriose, maltotetraose, maltopentaose, and maltoheptaose. The enzyme displays a greater affinity for longer maltooligosaccharides and is inactive on maltose. This enzyme's pH and temperature optima were determined to be 7.0 and 40°C, respectively. The enzyme's activity is not dependent on the presence of metal cations. Instead, metal cations such as mercury (Hg^{2+}) and copper (Cu^{2+}) inhibit its activity.[13]

Along with MTSase in *Arthrobacter* sp. Q36, researchers have characterized the activities of MTSases in several species of thermoacidophilic archaea, including *S. solfataricus* KM1, *S. acidocaldarius,* and *S. tokodaii*. These enzymes are also active on maltooligosaccharides, catalyzing an intramolecular transglycosylation reaction.[4,6,8] However, evidence from these studies suggests that MTSases may catalyze the hydrolysis of maltooligosaccharides and intermolecular transglycosylation as side reactions.[4,8]

In addition to evaluating their enzymatic activity, researchers have characterized the crystal structures of several *Sulfolobus* MTSases. In 2003, Kobayashi et al. published their structural characterization of the MTSase from *S. acidocaldarius* (SaMTSase). As shown in Fig.

2, the overall structure of this enzyme consists of three domains: A, B, and C. Domain A contains a $(\beta / \alpha)_8$-barrel structure similar to that of α-amylase family enzymes.[17] The $(\beta / \alpha)_8$-barrel, also known as the triosephosphate isomerase (TIM)-barrel, contains an eightfold repeat of (β-strand/α-helix) units, resulting in eight parallel β-strands at the enzyme's core, surrounded by eight α-helices.[18] The $(\beta / \alpha)_8$-barrel observed in SaMTSase lacks an α-helix between β-strands five and six and is considered incomplete. Along with the $(\beta / \alpha)_8$-barrel, domain A of SaMTSase contains two subdomains. Subdomain 1, located between the sixth β-strand and sixth α-helix of the barrel, contains eight α-helices. Subdomain 2, situated between the seventh β-strand and seventh α-helix of the barrel, contains five α-helices.[17]

Domain B extends from the third β-strand of the barrel and connects back to the third α-helix. This domain consists of three α-helices and four β-strands. The active-site cleft of SaMTSase is formed by domains A and B and includes the catalytic amino acids D228, E255, and D443, frequently conserved in α-amylase family enzymes. Finally, domain C is located at the C-terminus and consists of an eight-stranded anti-parallel β-sandwich.[17] Similar overall structures have been observed in the MTSases from *S. shibatae* DSM5389 and *S. tokodaii*.[7,9]

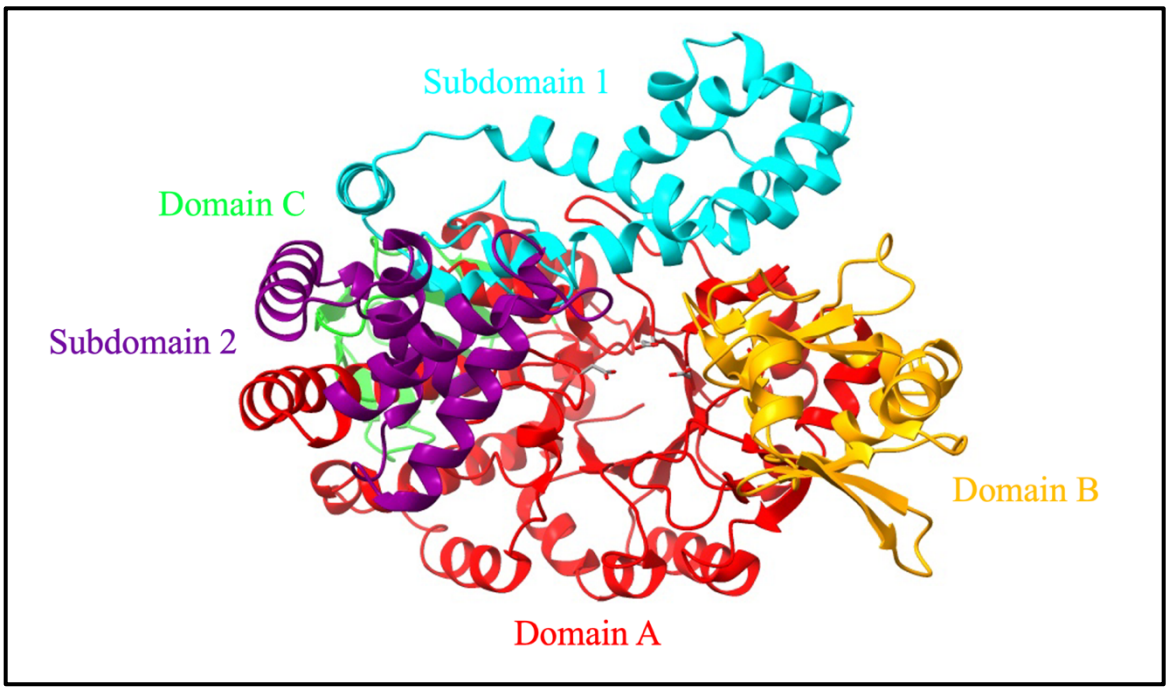

Fig. 2. MTSase from *Sulfolobus acidocaldarius* (UniProt: Q53688, PDB: 1IV8).[17] Domains and subdomains are separately colored and labeled. The side chains of the three catalytic residues (D228, E255, and D443) are shown at the center of the $(\beta/\alpha)_8$-barrel and colored by element. This illustration was produced using UCSF ChimeraX.[19,20]

Along with their structural characterization of SaMTSase, Kobayashi et al. proposed a mechanism of catalysis for MTSase enzymes. It is proposed that once MTSase binds the substrate (maltooligosaccharide), the sub-site -1 glucose ring is contorted by hydrogen bonds formed with one of the catalytic amino acids (D443 in SaMTSase). Subsequently, the other two catalytic residues (D228 and E255 in SaMTSase) function as acid and base catalysts, cleaving the α-1,4-glycosidic linkage. Finally, amino acids surrounding the active site facilitate the rotation of the cleaved glucose monomer, which is then reattached to form the α-1,1-glycosidic linkage.[17]

Maltooligosyl Trehalose Trehalohydrolase

Along with MTSases, maltooligosyl trehalose trehalohydrolases (MTHases) are also classified into the GH13 family. The activities of MTHases from several species, including *Arthrobacter* sp. Q36 and *S. acidocaldarius* have been experimentally characterized. These enzymes catalyze the hydrolysis of the α-1,4-glycosidic linkage that connects the maltooligosyl and trehalose moieties of maltooligosyl trehaloses. They are active on multiple substrates, including maltosyl trehalose, maltotriosyl trehalose, maltotetraosyl trehalose, and maltopentaosyl trehalose. Like MTSases, these enzymes prefer substrates with a higher degree of polymerization. The MTHase from *Arthrobacter* sp. Q36 functions optimally at a pH of 6.5 and 45°C. In contrast, the MTHase from *S. acidocaldarius*, a thermoacidophile, functions optimally within a pH range of 5.5-6.0 and at 75°C. The MTHases from both species are inhibited by metal cations such as mercury (Hg^{2+}), copper (Cu^{2+}), Iron (Fe^{2+}), and zinc (Zn^{2+}).[11,14]

Along with characterizing their activity, researchers have characterized the crystal structures of some MTHases. In 2000, Feese et al. published their characterization of the crystal structure of the MTHase from *S. solfataricus* KM1 (SsMTHase). This enzyme is a symmetric homodimer linked by a disulfide bond at residue C298. As shown in Fig. 3, each monomer consists of three major domains: A, C, and E. Domain A is the catalytic domain, consisting of a $(\beta/\alpha)_8$-barrel, along with two insertions (subdomains B and D). The subdomains form a hydrophobic trench that leads to the active site at the center of the $(\beta/\alpha)_8$-barrel. The active site contains the catalytic amino acids D252, E283, and D377, conserved in other GH13 family members. Domain C (C-terminal domain) consists of a γ-crystallin-type fold with a five-stranded anti-parallel β-sheet. Domain E (N-terminal domain) consists of a 7-stranded anti-parallel β-sandwich with an immunoglobulin-like Greek key topology. While similar domains are known

to serve as non-catalytic saccharide-binding domains in other glycosidases, domain E of SsMTHase lacks exposed tryptophan and proline residues typical of saccharide-binding surfaces. Thus, the function of domain E is unclear.[10]

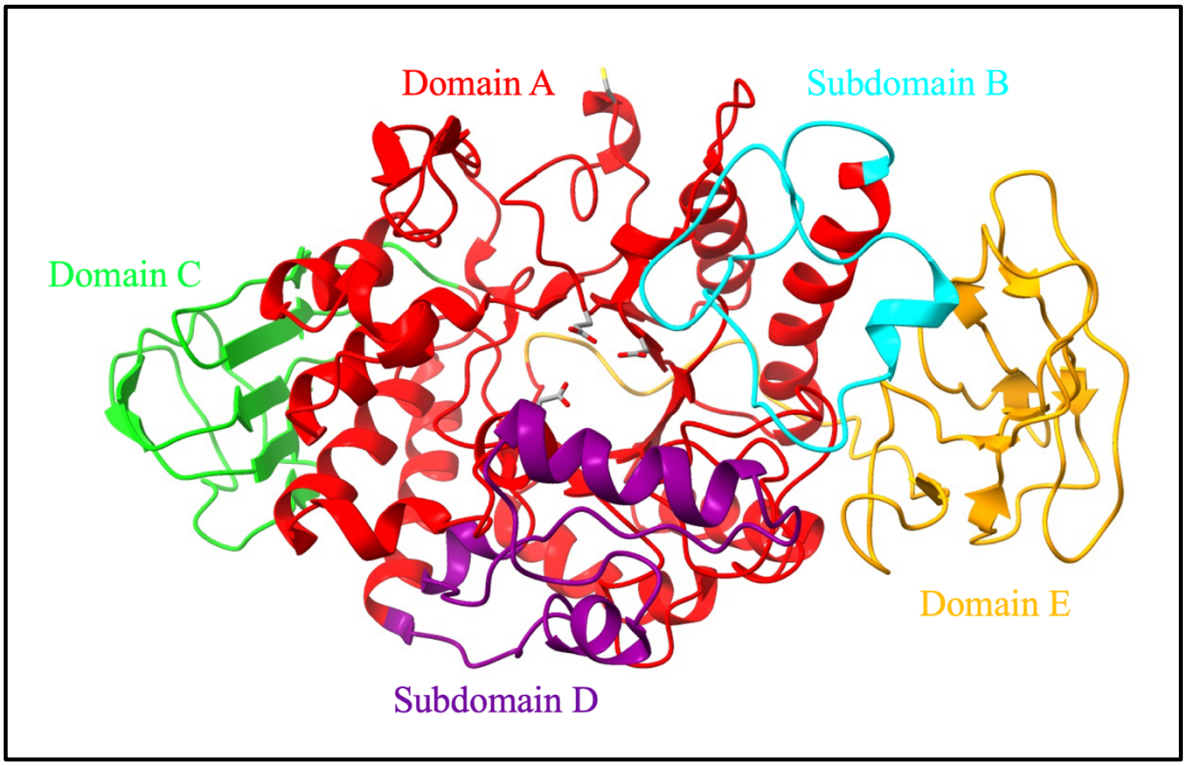

Fig. 3. MTHase from *Sulfolobus solfataricus* KM1 (UniProt: Q55088, PDB: 1EH9).[10] Domains and subdomains are separately colored and labeled. The side chains of the three catalytic residues (D252, E283, and D377) are shown at the center of the $(\beta/\alpha)_8$-barrel and colored by element. The side chain of residue C298, which allows for the formation of a symmetric homodimer, is shown at the top of the enzyme. This illustration was produced using UCSF ChimeraX.[19,20]

Additionally, the crystal structure of the MTHase from the bacterial extremophile *D. radiodurans* (DrMTHase) has been characterized. This enzyme is structurally like SsMTHase, consisting of the same domains. However, it lacks the cysteine residue involved in the dimerization of SsMTHase. Crystallization of DrMTHase in complex with trehalose revealed the

hydrogen bonding network and hydrophobic stacking interactions that recognize trehalose. Crystallization of DrMTHase in complex with maltose, which mimics a short maltooligosyl moiety, revealed an α-helix (residues 459-470) that undergoes a conformational change to hold maltose in the channel leading into the active site. This is accomplished through hydrogen bonds and hydrophobic stacking interactions between residues of DrMTHase and maltose. Overall, the catalytic mechanism of MTHases is believed to be like that of other GH13 family members. The catalytic residues (D275 and E308 in DrMTHase) serve as acid and base catalysts, allowing glycosidic bonds to be hydrolyzed.[15]

Salmonella typhimurium

The genus *Salmonella* contains two species: *S. enterica* and *S. bongori*. The former contains six subspecies, encompassing thousands of serovars differing in their flagellar, carbohydrate, and lipopolysaccharide structures.[21,22] *S. typhimurium* is a serovar of *S. enterica* subsp. *enterica*. This Gram-negative bacterial pathogen can be acquired by consuming contaminated food or water or through contact with infected animals or their feces.[21,23] *S. typhimurium* invades the intestinal wall of humans, causing illness that is typically self-limiting. Symptoms often include diarrhea, fever, and abdominal pain.[23] However, some strains of *S. typhimurium*, such as the multi-locus sequence type 313 (ST313) discovered in sub-Saharan Africa, can extend beyond the intestinal wall, colonize regions such as the liver and spleen, and cause systemic infection.[21,24] Compounding this, *S. typhimurium* is becoming increasingly antibiotic-resistant, posing a significant threat to global health and food safety.[25]

It is well-established that *S. typhimurium* can synthesize trehalose via the TPS/TPP pathway (also called the otsA/otsB pathway) previously described. Trehalose is involved in the response of *S. typhimurium* to abiotic stress. In 1996, Fang et al. found that an *otsA* mutant of *S.*

typhimurium strain 14028s had increased susceptibility to hyperosmotic stress compared to the wild-type strain. However, the mutant strain was not found to be more susceptible to heat stress. Additionally, this study found that the *otsA* mutant strain's virulence was not attenuated in mice when administered intraperitoneally (injected into the body cavity).[26] Similarly, Howells et al. found that an *otsA* mutant of *S. typhimurium* strain SL1344 had increased susceptibility to hyperosmotic stress but did not show attenuated virulence in mice when administered orally. However, this study differed from that of Fang et al. in that the *otsA* mutant was more susceptible to heat stress than the wild-type strain. Overall, these studies implicate the TPS/TPP pathway and trehalose in the environmental survival of *S. typhimurium* but not directly in its virulence.[27]

Central to the work described in this study, genes believed to encode an MTSase/MTHase trehalose biosynthetic pathway (*STM1559* and *STM1560*, respectively) were reported in *S. typhimurium* strain LT2 in 2001.[28] In 2004, Knuth et al. conducted a large-scale study using an insertion duplication mutagenesis approach to identify essential genes in *S. typhimurium*. They found that insertions into either *STM1559* or *STM1560* were lethal, preventing the growth of *S. typhimurium* under laboratory conditions.[29] However, the proteins encoded by these genes have never been computationally nor experimentally characterized. Research is needed to characterize these proteins for several reasons. First, determining this pathway to be functional would establish that *S. typhimurium* could biosynthesize trehalose via at least two pathways: TPS/TPP and MTSase/MTHase. Second, this would be the first characterization of this pathway in any species of Proteobacteria and in the pathogenic genus *Salmonella*. Finally, if this pathway is essential for *S. typhimurium* growth, as suggested by

Knuth et al., characterizing it could lead to the development of novel therapeutics to combat this bacterial pathogen.[29]

This study aimed to characterize the putative MTSase/MTHase trehalose biosynthetic pathway identified in *S. typhimurium*. First, comparative sequence and structural analysis of the putative StMTSase and StMTHase was performed to identify features conserved with functional homologs. Both enzymes retain all the amino acids required for catalysis and are similar in overall architecture to functional homologs. Both enzymes also contain largely conserved substrate binding sites, although a tyrosine cluster identified in most other characterized MTSases and believed to contribute to the +1 sub-site (see Fig. 1 for a review of sub-site nomenclature) is only partially conserved in the StMTSase. Specifically, StMTSase contains two residues (M460 and V464) that reside in this +1 sub-site and are non-conserved with the tyrosine residues found in other characterized homologs.

Second, the StMTSase was overexpressed, purified from *E. coli*, and biochemically characterized using a modified version of the Nelson-Somogyi (NS) method for detecting reducing sugars.[30] StMTSase was catalytically active on maltohexaose and dextrin but not maltotriose. The enzyme's pH and temperature optima were determined to be 7.0 and 40°C. The greatest activity was observed in the presence of potassium, whereas the presence of bovine serum albumin (BSA) decreased the enzyme's activity.

Finally, two mutant StMTSases were produced using site-directed mutagenesis to investigate the importance of two non-conserved amino acids. One mutant contained two substitutions of tyrosine (M460Y and V464Y) to match the binding site amino acids of characterized homologs and displayed no detectable activity. The other mutant contained a single substitution of tyrosine (M460Y) and displayed activity comparable to the wild-type enzyme.

This study is the first characterization of this pathway in any species of Proteobacteria, which includes many pathogenic genera, and provides evidence that the putative MTSase/MTHase trehalose biosynthetic pathway identified in *S. typhimurium* is functional. This work contributes to a better understanding of two reportedly essential *Salmonella* genes, whose products could potentially become the target of novel therapeutics.

CHAPTER TWO: MATERIALS AND METHODS

Computational Characterization of StMTSase and StMTHase

To compare the amino acid sequences of the putative maltooligosyl trehalose synthase from *Salmonella typhimurium* (StMTSase) and the putative maltooligosyl trehalose trehalohydrolase from *S. typhimurium* (StMTHase) with functional homologs, multi-sequence alignments were created using Clustal Omega.[31] These alignments were colored using ESPript 3.0.[32]

Based on the multi-sequence alignments, the overall domain architectures of StMTSase and StMTHase were identified. UCSF ChimeraX was used to generate illustrations of their domain architectures and structural overlays of their binding sites with functional homologs.[19,20] The electrostatic surface potential of each protein was calculated using the Adaptive Poisson Boltzmann Solver (APBS) web server, and the surface of each protein was colored using UCSF ChimeraX.[19,20,33] The protein sequences and structures analyzed throughout this study were all obtained from UniProt, the Protein Data Bank (PDB), or AlphaFold.[34,35] They can be retrieved using the accession codes listed in Tables 1 and 2.

Table 1. MTSase sequence and structure accession codes.

MTSase	UniProt ID	Structure ID
Sulfolobus acidocaldarius	Q53688	PDB: 1IV8
Salmonella typhimurium	Q8ZPF1	AlphaFold: AF-Q8ZPF1-F1
Sulfolobus tokodaii	Q973H2	PDB: 3HJE
Sulfolobus shibatae	Q7LYV2	PDB: 5ZCR
Arthrobacter sp. Q36	Q44315	AlphaFold: AF-Q44315-F1

Table 2. MTHase sequence and structure accession codes.

MTHase	UniProt ID	Structure ID
Sulfolobus solfataricus	Q55088	PDB: 1EH9

Salmonella typhimurium	Q8ZPF0	PDB: 3M07
Sulfolobus acidocaldarius	Q53641	AlphaFold: AF-Q53641-F1
Arthrobacter sp. Q36	Q44316	AlphaFold: AF-Q44316-F1
Deinococcus radiodurans	Q9RX51	PDB: 2BHU
Deinococcus radiodurans (in complex with trehalose)	Q9RX51	PDB: 2BHY
Deinococcus radiodurans (in complex with maltose)	Q9RX51	PDB: 2BHZ

Site-Directed Mutagenesis

The Center for Structural Genomics of Infectious Diseases (CSGID) provided the pMcSGJ3 plasmid, which encodes the putative StMTSase in fusion with a polyhistidine tag (plasmid information is provided in Table A3). Site-directed mutagenesis was used to generate two mutant enzymes containing substitutions introducing tyrosine to more closely match the binding site amino acids identified in known functional MTSases. The StMTSase-M460Y-V464Y mutant contains two substitutions introducing tyrosine (M460Y and V464Y), while the StMTSase-M460Y mutant contains a single substitution introducing tyrosine (M460Y).

To generate the StMTSase-M460Y-V464Y mutant, PCR was performed using the pMcSGJ3 plasmid as the template, and the primers SDM1F and SDM1R, which were designed to make the M460Y and V464Y mutations (primer and plasmid information are provided in Tables A1 and A3). The PCR reaction consisted of 40.7 μL of water, 12 μL of 5x Phusion High-Fidelity reaction buffer, 1.25 μL of 25 ng/μL pMcSGJ3 template, 1.0 μL of 10 μM forward primer, 1.0 μL of 10 μM reverse primer, 1.2 μL of 10 mM dNTP mix, 1.0 μL of Phusion Hot Start II DNA polymerase, and 1.8 μL of DMSO. A gradient PCR was performed to determine the optimal primer annealing temperature. The 60 μL PCR reaction was divided into 6 PCR tubes. PCR was performed using the following annealing temperatures: 55°C, 58.3°C, 61.4°C,

65.2°C, 68.8°C, and 72°C. The thermocycler settings used were 98°C for 30 s, (98°C for 15 s, temperature gradient for 30 s, 72°C for 9 min) x19 cycles, 72°C for 10 min.

To generate the StMTSase-M460Y mutant, PCR was performed using the pMcSGJ3 plasmid as the template, and the primers SDM2F and SDM2R, which were designed to make the M460Y mutation (primer and plasmid information are provided in Tables A1 and A3). The PCR reaction consisted of 32 μL of water, 10 μL of 5x Phusion High-Fidelity reaction buffer, 3 μL of 25 ng/μL pMcSGJ3 template, 0.75 μL of 10 μM forward primer, 0.75 μL of 10 μM reverse primer, 1.0 μL of 10 mM dNTP mix, 1.0 μL of Phusion Hot Start II DNA polymerase, and 1.5 μL of DMSO. A gradient PCR was performed to determine the optimal primer annealing temperature. The 50 μL PCR reaction was divided into 5 PCR tubes. PCR was performed using the following annealing temperatures: 40°C, 41°C, 45.8°C, 51.9°C, and 55°C. The thermocycler settings used were 98°C for 3 min, (98°C for 30 s, temperature gradient for 30 s, 72°C for 3 min) x35 cycles, 72°C for 10 min.

Agarose Gel Electrophoresis

Agarose gel electrophoresis was used to identify the presence of PCR products following site-directed mutagenesis. A 1% agarose gel was cast. Once solidified, the gel was placed in a gel rig and covered with Tris-acetate-EDTA (TAE) buffer (Table A5). To prepare the samples, 2 μL of PCR product was mixed with 1 μL of 6x loading dye (Table A5) and 3 μL of water. 5 μL of each sample was loaded into separate wells of the gel. One well contained 5 μL of the GeneRuler 1 kb Plus DNA ladder. The gel was subjected to 100 V for 30 min and then stained overnight with 3x Gel Green. Finally, the gel was viewed using a blue light transilluminator. This protocol was used for all agarose gel electrophoresis performed in this study.

Bacterial Transformation

Using the following protocol, the mutant plasmids produced via site-directed mutagenesis were transformed into DH5α and BL21 *E. coli* cells (bacterial strain information is provided in Table A2). First, 0.5 μL of Dpn1 restriction endonuclease was added to the PCR product and incubated at room temperature for 15 min. This allowed the template DNA, which does not contain the desired mutation(s), to be degraded. Meanwhile, 250 μL of competent *E. coli* cells (DH5α or BL21) were removed from -80°C storage and thawed on ice. Once thawed, 5 μL of PCR product was added to the cells and incubated on ice for 30 min. The cells were heat shocked in a 42°C water bath for 1.5 min and then immediately placed back on the ice for 2 min.

Subsequently, 500 μL of S.O.C. outgrowth medium (Table A5) was added to the cells. The cells were then incubated for 45 min at 37°C while shaking at 250 rpm. After incubation, the cells were pelleted via centrifugation (13,300 rpm, 30 s). Most of the supernatant was discarded, and the cells were pipetted up and down to resuspend them in the remaining S.O.C. outgrowth medium. Finally, the cells were spread onto agar plates containing lysogeny broth (LB) and ampicillin. The plates were sealed with parafilm and incubated overnight at 37°C.

Plasmid DNA Isolation

Plasmid DNA was produced using DH5α *E. coli* cells, isolated, and sent for sequencing to confirm that the desired mutation(s) were present. A 3 mL liquid culture of *E. coli* containing mutant plasmid DNA was grown in autoclaved 25 g/L LB (Table A5) along with 3 μL of 100 mg/mL filter-sterilized ampicillin. The culture was allowed to grow overnight at 37°C while shaking at 250 rpm. The next day, the tube was swirled to ensure that all cells were suspended, and 1.5 mL of the cell suspension was added to a 1.5 mL Eppendorf tube. The tube was capped and centrifuged (13,300 rpm, 30 s) to pellet the cells. The supernatant was discarded, and the

tube was vortexed to resuspend the bacterial pellet in the remaining small amount of LB. Then, 100 μL of miniprep solution 1 (Table A5) and 1 μL of RNaseA were added to the tube. The tube was then vortexed to resuspend the cells.

Once all the cells were resuspended, 200 μL of miniprep solution 2 (Table A5) was added to the tube. The tube was capped, inverted multiple times to mix the solution, and placed on ice for 5 min. Next, 150 μL of ice-cold miniprep solution 3 (Table A5) was added to the tube. Again, the tube was capped, inverted multiple times to mix, and placed on ice for 5 min. The tube was then centrifuged (13,300 rpm, 5 min).

Once the tube had been centrifuged, 450 μL of the supernatant was pipetted into a clean, 1.5 mL Eppendorf tube. An equal volume of isopropanol was then added to the supernatant. The tube was capped, inverted multiple times to mix, and allowed to sit at room temperature for 2 min. Next, the tube was centrifuged (13,300 rpm, 5 min) to pellet the plasmid DNA. The supernatant was carefully discarded, and 200 μL of 100% ethanol was added to the tube. The tube was inverted multiple times to mix and then centrifuged again (13,300 rpm, 2 min). The ethanol was discarded, and a pipette was used to remove as much of it as possible without dislodging the plasmid DNA pellet. The tube was then left open and inverted on a kimwipe to allow any traces of ethanol to evaporate.

Once all the ethanol had evaporated, 25 μL of nuclease-free water was added to the tube. The solution was pipetted up and down several times to resuspend the plasmid DNA pellet. Then, an approximate plasmid DNA concentration was determined using a NanoDrop microvolume spectrophotometer. To confirm the presence of the desired mutation(s), 50 μL of an approximate 150 ng/μL plasmid DNA solution was sent to Eurofins Genomics for sequencing.

Overexpression and Purification of StMTSases

Wild-type StMTSase, StMTSase-M460Y-V464Y, and StMTSase-M460Y were each overexpressed in BL21 *E. coli* cells and purified using immobilized metal affinity chromatography (IMAC). A starter culture of BL21 *E. coli* cells containing a plasmid encoding wild-type StMTSase (or one of the mutant StMTSases) in fusion with a polyhistidine tag was grown in 10 mL of autoclaved 25 g/L LB (Table A5) along with 10 μL of 100 mg/mL filter-sterilized ampicillin. The starter culture was grown overnight at 37°C while shaking at 250 rpm. The next day, the starter culture was added to 1 L of autoclaved 25 g/L LB along with 1000 μL of 100 mg/mL filter-sterilized ampicillin. The 1 L culture was then grown at 37°C while shaking at 250 rpm until the optical density at 600 nm (OD_{600}) reached 0.4, as measured by a spectrophotometer. Once an OD_{600} of 0.4 was reached, a 20 μL culture sample was obtained for SDS-PAGE. Then, 1000 μL of 1 M isopropyl β-D-1-thiogalactopyranoside (IPTG) was added to the liquid culture. The liquid culture was then grown overnight at 21°C while shaking at 250 rpm.

The next day, the BL21 *E. coli* cells were harvested by centrifugation (7000 xg, 15 min, 4°C). The supernatant was removed, and the *E. coli* cells were resuspended in 40 mL of 1x binding buffer (Table A5) along with two Pierce Protease Inhibitor Mini Tablets (ThermoFisher Catalog # A32956). The resuspended cells remained on ice and were lysed via 8 rounds of sonication. Each round consisted of 30 s of sonication followed by 1 min of rest to prevent heating the protein. A 20 μL sample of the lysate was obtained for SDS-PAGE. The lysate was then centrifuged (10,000 xg, 30 min, 4°C). The supernatant containing StMTSase was transferred into a clean 50 mL conical tube along with 2 mL of a 50% nickel bead solution. The tube was placed on a shaker in a cold room for 1.5 h to allow the protein to bind the nickel beads.

Separately, the pelleted insoluble fraction was resuspended in 40 mL of deionized water, and a 20 μL sample was taken for SDS-PAGE.

After shaking for 1.5 h, the tube was centrifuged (3000 rpm, 5 min, 4°C), and the unbound supernatant fraction was gently removed with a pipette. A 20 μL sample was taken for SDS-PAGE, and the rest was discarded. Another 25 mL of 1x binding buffer was added to the tube. The tube was mixed well and centrifuged again (3000 rpm, 5 min, 4°C). Again, the supernatant was gently removed with a pipette and discarded. The nickel beads, which StMTSase was bound to, were pipetted into a protein purification column and placed in a cold room. Excess binding buffer was allowed to flow through the column into a clean beaker, and a 20 μL sample was taken for SDS-PAGE. Meanwhile, 20 mL of 1x wash buffer (Table A5) was added to the tube, which was then inverted several times to capture any residual beads that were not transferred into the column. The wash buffer was then allowed to flow through the column into a clean beaker, and a 20 μL sample was taken for SDS-PAGE. Subsequently, 10 mL of 1x elution buffer (Table A5) was added to the column. The elution flowed through the column, was collected in a clean beaker, and kept on ice. A 20 μL sample of the elution was taken for SDS-PAGE.

Approximately 9 cm of Spectra/Por 1 dialysis tubing (Part # 132650, Molecular weight cutoff: 6-8 kDa) was placed in 1 L of pH 7.0 dialysis buffer (Table A5) to hydrate. Once hydrated, one end of the dialysis tubing was clipped, and the protein elution was pipetted into the tubing. Once the elution had been added, the other end of the dialysis tubing was clipped, and the tubing was placed back into 1 L of dialysis buffer. The elution was dialyzed overnight in a cold room with gentle stirring using a magnetic stir bar. The next day, the dialysis tubing (containing the purified protein) was moved into 1 L of fresh dialysis buffer and dialyzed for another 3 h in a

cold room. Finally, the purified protein was pipetted from the dialysis tubing into a 15 mL conical tube and kept on ice. A 20 μL sample of the purified protein was taken for SDS-PAGE. The remaining protein was aliquoted into 1.5 mL Eppendorf tubes and frozen at -20°C.

SDS-PAGE

Sodium dodecyl sulfate-polyacrylamide gel electrophoresis (SDS-PAGE) was used to detect the presence of proteins in aliquots taken throughout the protein purification process and StMTSase in the purified protein stocks. A 10% Tris-glycine reducing SDS-PAGE gel was cast using the reagents shown in Table 3 (components of the upper and lower buffers are in Table A5). Samples to be analyzed were mixed with an equal volume of 2x SDS-PAGE sample buffer (Table A5) and put in a boiling water bath for 3 min. Once boiled, 12.5 μL of each sample was loaded into separate gel wells. One well of the gel also contained 3.5 μL of PageRuler Plus protein ladder. The gel was submerged in a running buffer (Table A5) and subjected to 200 V for 45 min. The gel was then placed in Coomassie brilliant blue stain (Table A5) and stained overnight while shaking. The next day, the gel was placed in destain (Table A5) for 2 h before being viewed.

Table 3. Reagents used to cast SDS-PAGE gels.

Stacking (Upper) Gel	**Resolving (Lower) Gel**
3 mL water	4 mL water
1.25 mL 4x upper buffer	1.3 mL 8x lower buffer
0.75 mL acrylamide	3.3 mL acrylamide
60 μL 5% APS	1.3 mL 75% sucrose
15 μL TEMED	100 μL 5% APS
	6 μL TEMED

Determination of StMTSase Concentration

A Bradford assay was used to determine the concentration of StMTSase in the purified protein stocks. Bovine serum albumin (BSA) standards ranging from 0 mg/mL to 0.25 mg/mL were prepared. Then, 10 μL of each standard was pipetted into individual wells of a clear, round bottom 96-well plate in duplicate. Serial dilutions of the StMTSase stocks were made, and 10 μL of each was added to individual wells of a 96-well plate in duplicate. Next, 200 μL of Coomassie Plus Reagent was added to all wells. The 96-well plate was shaken to mix and incubated at room temperature for 10 min. Each well's absorbance (595 nm) was measured with a microplate spectrophotometer. The absorbances of duplicates were averaged. A linear BSA standard curve was produced and used to calculate the concentration of StMTSase in the purified protein stocks.

Quantification of StMTSase Activity

StMTSase activity was assessed using a modified version of the Nelson-Somogyi (NS) assay, a colorimetric assay for detecting reducing sugars.[30] This is because MTSases convert reducing maltooligosaccharides into the non-reducing saccharide maltooligosyl trehalose. Enzymatic reactions proceeded for 45 min (although the reaction conditions varied depending on the experiment and are detailed below) and were stopped using a boiling water bath for 3 min. Controls consisted of the same components as the enzymatic reactions but went immediately into a boiling water bath for 3 min upon adding the enzyme.

Once all reactions had been stopped using a boiling water bath, all the tubes were centrifuged (13,300 rpm, 10 min) to capture condensation. If necessary, all tubes were diluted equally to ensure the final substrate concentrations were within the linear range of the assay (approximately 0 mM to 1 mM).[30] Next, 45 μL of each enzymatic reaction (or control) was pipetted into separate wells of a polypropylene 96-well plate. Then, 45 μL of working reagent

(Table A5) was added to each well. The plate was then covered with a microplate seal and wrapped tightly in aluminum foil to prevent water from entering. The sealed plate was placed in a boiling water bath for 25 min. After boiling, the plate was placed in a Ziplock bag and cooled under cold, running water for 5 min.

After cooling, the plate was removed from the aluminum foil. A needle was used to poke a hole in the microplate seal over each well to release pressure. Still sealed, the plate was centrifuged (3,500 rpm, 15 min) to capture condensation. The microplate seal was removed, and 45 μL of color reagent (Table A5) was added to each well. Each well was mixed by pipetting up and down. 100 μL from each well was then transferred into separate wells of a clear, flat-bottomed 96-well plate. The absorbance (600 nm) of each well was measured using a microplate spectrophotometer. The absorbances of duplicates were averaged. In most cases, enzyme activity was assessed by subtracting the average reaction absorbance from the average control absorbance (the decrease in absorbance is proportional to the amount of substrate consumed) and then dividing by the amount of enzyme (mg) and time (45 min), yielding units of ΔAbs mg^{-1} min^{-1}. To investigate the effects of maltohexaose concentration on the reaction rate and attempt to obtain a Michaelis-Menten saturation curve, a maltohexaose standard curve was produced using the average absorbances of the controls. A change in maltohexaose concentration between the enzymatic reactions and controls was calculated from this standard curve and then divided by the amount of enzyme (mg) and time (45 min), yielding units of mmol mg^{-1} min^{-1}.

Temperature-Dependence Assay

To determine the temperature optimum of StMTSase, a 2.00 mM maltohexaose solution, which served as the substrate, was first prepared in pH 7.0 McIlvaine buffer (Table A5).

Meanwhile, the following temperatures were achieved using water baths: 7°C, 20°C, 30°C, 37°C, 40°C, 47°C, and 57°C.

Enzymatic reactions at each temperature were performed in duplicate and consisted of 45 μL of purified StMTSase (0.036 mg) and 45 μL of the substrate in 1.5 mL Eppendorf tubes. The reactions were allowed to proceed for 45 min and then stopped using a boiling water bath for 3 min. Controls were also performed in duplicate and consisted of the same components but went straight into a boiling water bath for 3 min after adding StMTSase. StMTSase activity was then assessed using the NS assay previously described.

pH-Dependence Assay

To determine the optimal pH for StMTSase, several buffers were first made. McIlvaine buffers (Table A5) were prepared and adjusted to pHs of 4.0, 4.96, 6.15, and 7.05. Tris-HCl buffers (Table A5) were prepared and adjusted to pHs of 7.94 and 8.94. Finally, sodium carbonate and sodium bicarbonate solutions were prepared (Table A5). Appropriate volumes of each were mixed to produce sodium carbonate bicarbonate buffers with pHs of 9.60 and 10.94. The pH of each buffer was adjusted using HCl and NaOH and monitored using a calibrated pH probe.

A 10.04 mM maltohexaose stock solution was prepared in deionized water. Portions of this stock solution were then diluted with the buffers previously described to yield 1.13 mM maltohexaose substrate solutions with pHs ranging from 4.0 to 10.94. Enzymatic reactions at each pH were performed in duplicate and consisted of 10 μL of purified StMTSase (0.031 mg) and 80 μL of the substrate in 1.5 mL Eppendorf tubes. The reactions were allowed to proceed for 45 min at 40°C and were then stopped using a boiling water bath for 3 min. Controls consisted of

the same components but went directly into a boiling water bath for 3 min after adding StMTSase. StMTSase activity was then quantified using the NS assay previously described.

Assay of Potential Activators

To assess whether potassium or bovine serum albumin (BSA) could enhance StMTSase activity, a 4.6 mM maltohexaose solution was prepared in pH 7.0 McIlvaine buffer (Table A5) and served as the substrate. Similarly, 2.1 mM KCl and 4.2 mg/mL bovine serum albumin (BSA) solutions were separately prepared in the same buffer. Duplicate enzymatic reactions and corresponding controls were set up in 1.5 mL Eppendorf tubes, as shown in Table 4. The total reaction volume remained at 70 μL. The final maltohexaose concentration in each reaction was 2.96 mM. Reactions containing KCl contained a final concentration of 300 mM, while reactions containing BSA contained a final concentration of 0.6 mg/mL.

The enzymatic reactions proceeded for 45 min at 40°C and were stopped using a boiling water bath for 3 min. Controls went directly into a boiling water bath for 3 min after adding StMTSase. StMTSase activity was then quantified using the NS assay previously described.

Table 4. Experimental setup used to assess the effects of potassium and BSA on StMTSase.

	Maltohexaose (μL)	**Enzyme (μL)**	**McIlvaine Buffer (μL)**	**KCl (μL)**	**BSA (μL)**
McIlvaine Buffer Only	45	5	20	0	0
+ 300 mM KCl	45	5	10	10	0
+ 0.6 mg/mL BSA	45	5	10	0	10
+ 300 mM KCl and 0.6 mg/mL BSA	45	5	0	10	10

Assay of the Reaction Rate vs. Maltohexaose Concentration

The StMTSase reaction rate was also evaluated across increasing substrate concentration. Maltohexaose in pH 7.0 McIlvaine buffer containing 300 mM KCl (Table A5) was used as the substrate. Maltohexaose concentrations ranging from 2.5 mM to 25 mM were prepared by serial dilution. Duplicate enzymatic reactions and controls were set up in 1.5 mL Eppendorf tubes and contained 45 μL of the substrate and 5 μL of the enzyme (.00391 mg). The enzymatic reactions proceeded for 45 min at 40°C and were stopped using a boiling water bath for 3 min. Controls went directly into a boiling water bath for 3 min after adding StMTSase. StMTSase activity was then quantified using the NS assay previously described.

Assay of Mutant StMTSases

The activities of two mutant StMTSases produced by our laboratory (StMTSase-M460Y-V464 and StMTSase-M460Y) were assessed alongside the wild-type enzyme. A 3.0 mM maltohexaose solution in pH 7.0 McIlvaine buffer containing 300 mM KCl (Table A5) was used as the substrate. Enzymatic reactions contained 45 μL of the substrate and 5 μL of the appropriate enzyme in 1.5 mL Eppendorf tubes. The reactions proceeded at 40°C for 45 min and were stopped using a boiling water bath. Control reactions contained the same components and went immediately into a boiling water bath upon adding the enzyme. StMTSase activity was then quantified using the NS assay previously described.

CHAPTER THREE: RESULTS

Computational Characterization of StMTSase

Maltooligosyl trehalose synthases (MTSases) have mostly been studied in archaea, with those from *Sulfolobus acidocaldarius*, *Sulfolobus tokodaii*, and *Sulfolobus shibatae* having solved crystal structures.[7,9,17] These structures have improved our understanding of the amino acids important for MTSase function. Thus, we sought to compare the sequence of the putative MTSase from *Salmonella typhimurium* (StMTSase) to these characterized homologs to identify the conservation of important amino acids and to identify any unique differences. Additionally, while no crystal structure exists for StMTSase, an AlphaFold model was compared to the solved structures of these homologs to identify structural similarities and differences. The AlphaFold model of StMTSase, along with the predicted confidence, is shown in Fig. 4.[34,35]

A multi-sequence alignment containing StMTSase and functional homologs was created using Clustal Omega and colored using ESPript 3.0.[31,32] This alignment includes known functional MTSases from the following organisms: *S. acidocaldarius* (UniProt: Q53688), *S. tokodaii* (UniProt: Q973H2), *S. shibatae* B12 (UniProt: Q7LYV2), and *Arthrobacter* sp. Q36 (UniProt: Q44315). Structural analysis of the StMTSase AlphaFold model (AF-Q8ZPF1-F1) was conducted using UCSF ChimeraX.[19,20,34,35]

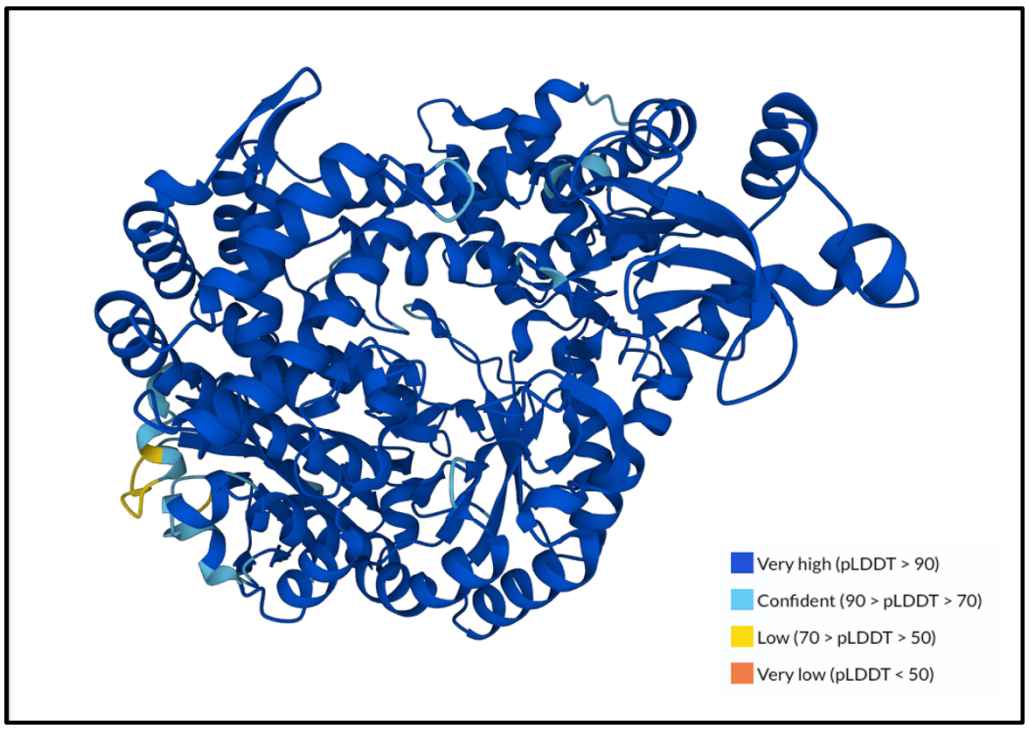

Fig. 4. AlphaFold confidence model for StMTSase (UniProt: Q8ZPF1, AlphaFold: AF-Q8ZPF1-F1). The structure of StMTSase predicted by AlphaFold is shown. The protein is colored by confidence score (pLDDT), which is generated by AlphaFold and ranges from 0-100. Regions of the protein structure with a higher pLDDT are expected to be predicted with greater accuracy.[34,35]

As shown in Fig. 5 and 6, all three catalytic residues characteristic of glycoside hydrolase family 13 (GH13) enzymes are conserved in StMTSase (D251, E279, and D517). The residues Y51, D86, and R249 are sequentially and structurally conserved in StMTSase, corresponding to residues reported to surround the catalytic site and form a hydrogen-bond network in the MTSase from *S. acidocaldarius* (SaMTSase) and other GH13 enzymes. StMTSase also contains residues that form part of a putative +1 sub-site (see Fig. 1 for a review of sub-site nomenclature), which have been shown by mutational analysis to contribute to the enzyme activity of homologs. These include H252, D254, K280, K462, E465, D466, and K519.[7,17] Additionally, the binding site of StMTSase has an electrostatic surface potential that is largely negative. This is consistent with the SaMTSase binding site (Fig. 7).

In contrast, a tyrosine cluster believed to contribute to the +1 sub-site in SaMTSase is only partially conserved in StMTSase (Fig. 5 and 6). In SaMTSase, three amino acids (Y349, Y274, and H229) are proposed to form hydrogen bonds with the glucose monomer in the +1 sub-site before it is rotated 180° to convert the α-1,4-glycosidic linkage to an α-1,1-glycosidic linkage. These residues are all conserved in StMTSase and correspond to Y390, Y300, and H252, respectively. Five residues of SaMTSase are proposed to hydrogen bond with the glucose monomer following its rotation (H229, Y349, E393, K445, and Y392). The first four are sequentially and structurally conserved in StMTSase, as shown in Fig. 5 and 6, corresponding to H252, Y390, E465, and K519, respectively. However, Y392 of SaMTSase is not conserved in StMTSase and corresponds to V464. Additionally, the residue Y388 of SaMTSase, which lies in the +1 sub-site, is not conserved in StMTSase and corresponds to M460.[17]

The formation of more hydrogen bonds following a 180° rotation of the glucose monomer in the +1 sub-site is believed to stabilize this conformation and drive the formation of the α-1,1-glycosidic linkage that is characteristic of trehalose.[17] Thus, there is interest in uncovering whether the activity of StMTSase is affected by these non-conserved residues.

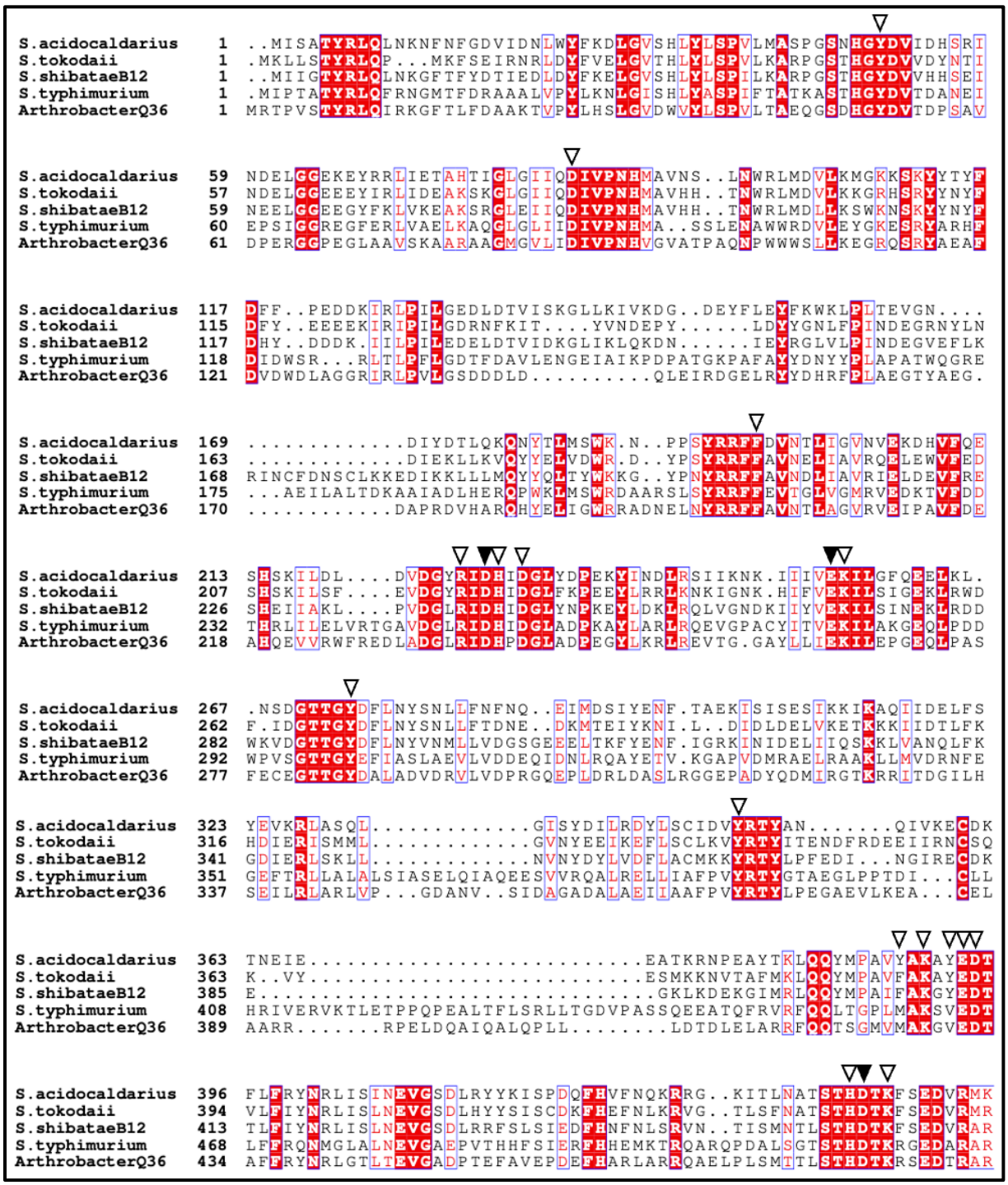

Fig. 5. Multi-sequence alignment of StMTSase and functional homologs. Catalytic residues are indicated with shaded triangles, while residues shown previously to be involved in substrate binding or enzyme activity are indicated with open triangles. Residues that are conserved among all the homologs in this alignment are shaded in red, while residues that are physiochemically conserved among all the homologs are outlined in blue. The following MTSase sequences were included in this alignment: *Salmonella typhimurium* (UniProt: Q8ZPF1), *Sulfolobus acidocaldarius* (UniProt: Q53688), *Sulfolobus tokodaii* (UniProt: Q973H2), *Sulfolobus shibatae*

B12 (UniProt: Q7LYV2), and *Arthrobacter* sp. Q36 (UniProt: Q44315). This alignment was created using Clustal Omega and colored using ESPript 3.0.[31,32]

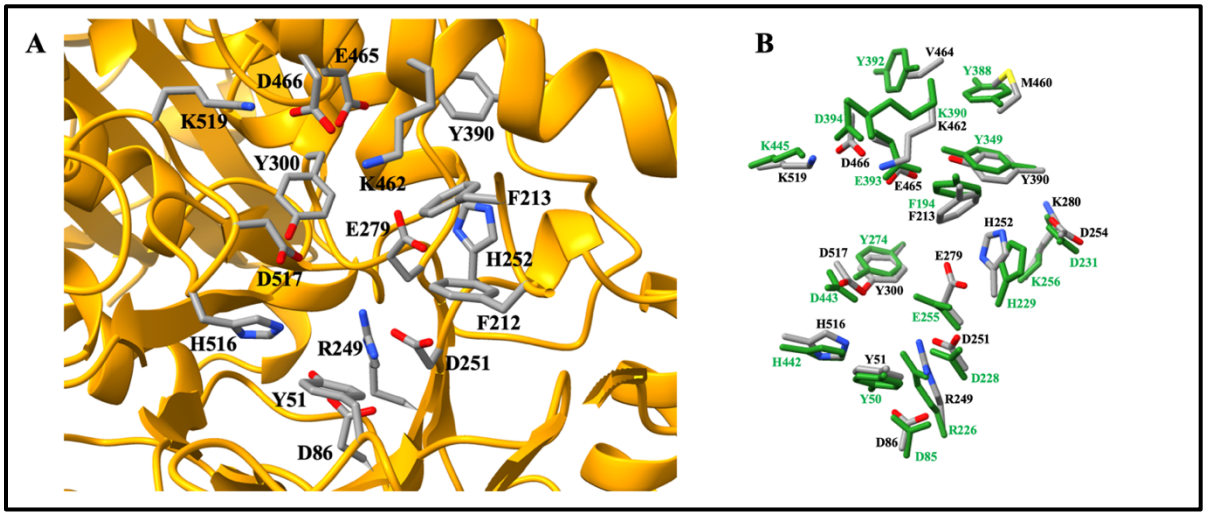

Fig. 6. Active site of StMTSase (UniProt: Q8ZPF1, AlphaFold: AF-Q8ZPF1-F1). (A) Residues in the active site are labeled, with their side chains shown and colored by element. The protein backbone is shown in orange. (B) The active site of StMTSase is overlayed with that of the *Sulfolobus acidocaldarius* MTSase (UniProt: Q53688, PDB: 1IV8).[17] The side chains of StMTSase residues are colored by element and labeled in black. The side chains of *S. acidocaldarius* MTSase residues are colored and labeled green. These illustrations were produced using UCSF ChimeraX.[19,20]

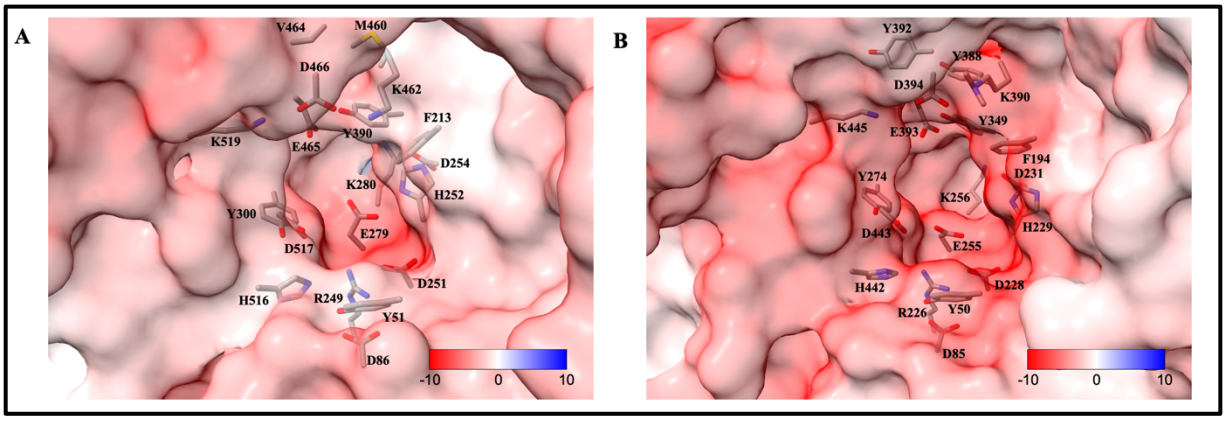

Fig. 7. Electrostatic surface potential of StMTSase (UniProt: Q8ZPF1, AlphaFold: AF-Q8ZPF1-F1). The electrostatic surface potentials of (A) the StMTSase binding site and (B) the binding site of the MTSase from *Sulfolobus acidocaldarius* (UniProt: Q53688, PDB: 1IV8) are shown.[17] The side chains of binding site amino acids are shown and colored by element. Regions of negative electrostatic potential are shown in red, whereas regions of positive electrostatic potential are shown in blue. The electrostatic surface potential of each protein was calculated

using the Adaptive Poisson Boltzmann Solver (APBS) web server.[33] These illustrations were produced using UCSF ChimeraX.[19,20]

As shown in Fig. 8, the sequence and structure analysis also revealed that StMTSase is structurally like the MTSases from *S. acidocaldarius* (Fig. 2), *S. shibatae* DSM5389, and *S. tokodaii*, and consists of the same three major domains. Domain A (M1-H91, M221-G745) is the catalytic domain and contains a $(\beta/\alpha)_8$-barrel structure. There are two insertions into the $(\beta/\alpha)_8$-barrel, referred to as subdomains 1 (L310-H489) and 2 (E522-L632). Domain B is an extension from domain A (M92-G220), while domain C is at the C-terminus (D746-D842). Domains A and B and the subdomains form the enzyme's active site. The conserved catalytic amino acids (D251, E279, and D517) are located at the center of the $(\beta/\alpha)_8$-barrel.

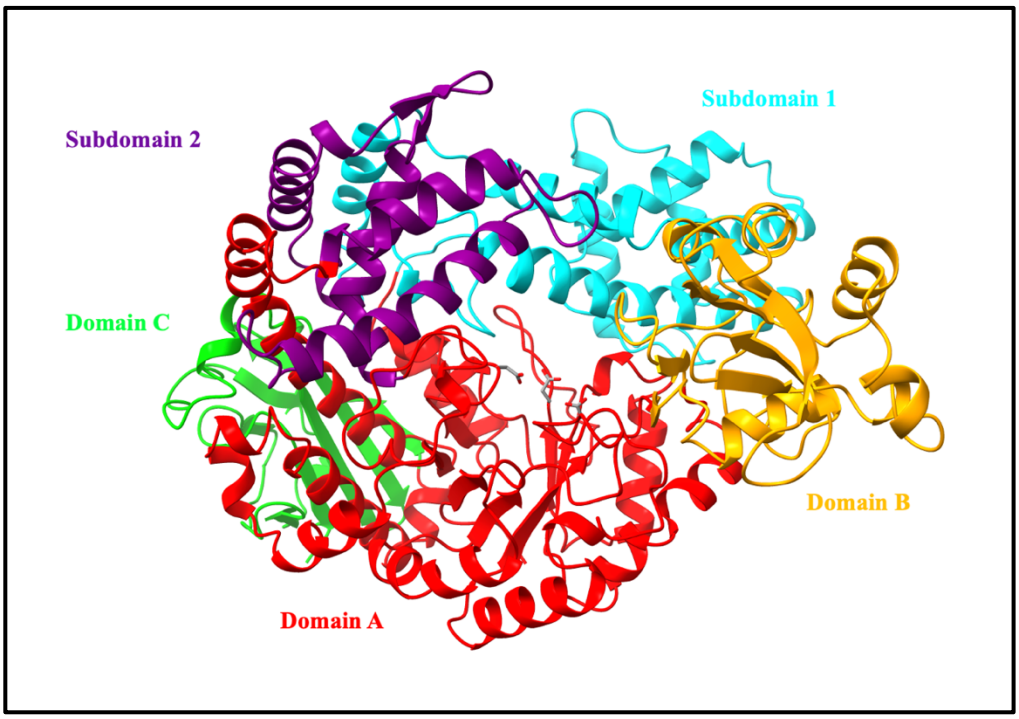

Fig. 8. Domain architecture of StMTSase (UniProt: Q8ZPF1, AlphaFold: AF-Q8ZPF1-F1). The major domains and subdomains of domain A are separately colored and labeled. The side chains of the three conserved catalytic residues (D251, E279, and D517) are shown and colored by

element at the center of the $(\beta/\alpha)_8$-barrel of domain A. This illustration was produced using UCSF ChimeraX.[19,20]

Computational Characterization of StMTHase

Along with MTSases, maltooligosyl trehalose trehalohydrolases (MTHases) have mostly been studied in extremophiles, with those from *Sulfolobus solfataricus* and *Deinococcus radiodurans* having solved crystal structures.[10,15] Thus, we sought to compare the sequence of the putative MTHase from *S. typhimurium* (StMTHase) to these characterized homologs to identify the conservation of important amino acids and any unique differences. Additionally, the structure of StMTHase at 1.4 Å resolution was experimentally determined by the Center for Structural Genomics of Infectious Diseases (CSGID) in 2010 (PDB: 3M07). Therefore, we sought to compare the crystal structure of StMTHase to the structures of these homologs to identify structural similarities and differences.

A multi-sequence alignment containing StMTHase and functional homologs was created using Clustal Omega and colored using ESPript 3.0.[31,32] This alignment includes known functional MTHases from the following organisms: *S. acidocaldarius* (UniProt: Q53641), *S. solfataricus* KM1 (UniProt: Q55088), *Arthrobacter* sp. Q36 (UniProt: Q44316), and *D. radiodurans* (UniProt: Q9RX51). As shown in Fig. 9, all three catalytic residues (D261, E296, and D393) characteristic of glycoside hydrolase family 13 (GH13) enzymes are conserved in StMTHase (shaded triangles).

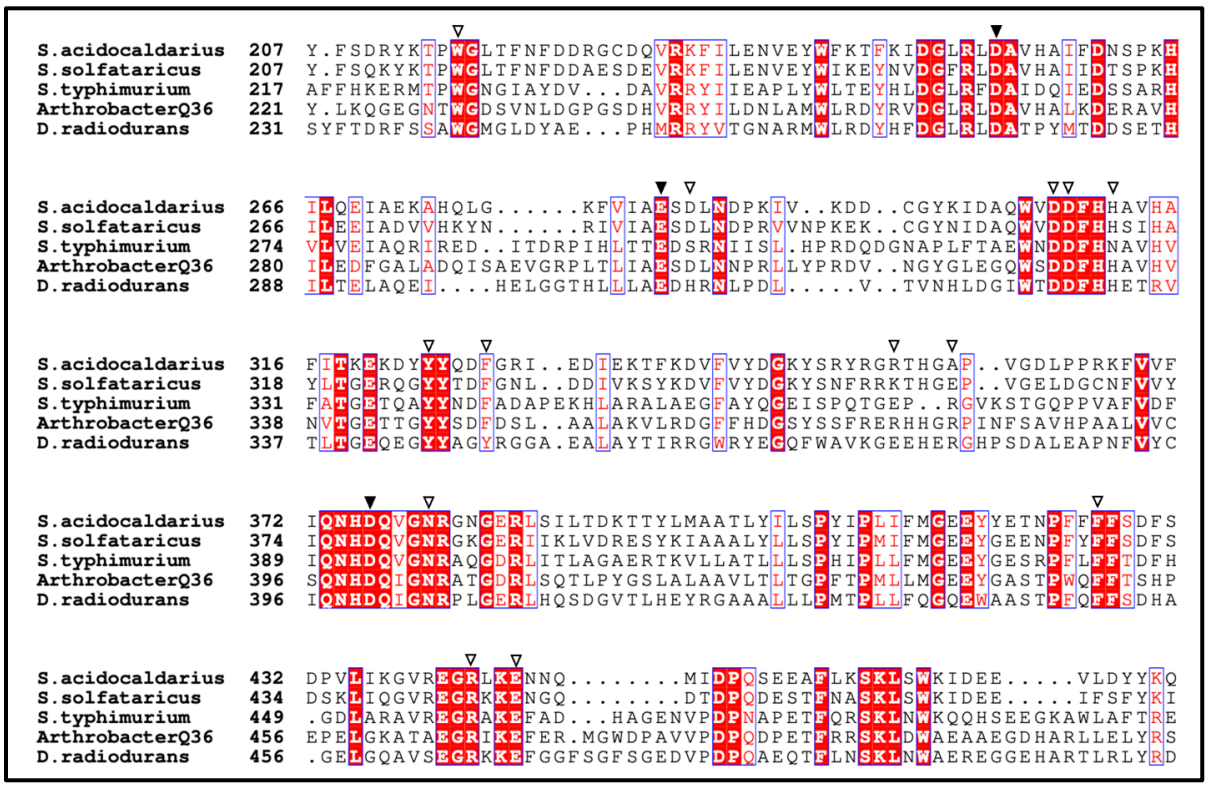

Fig. 9. Multi-sequence alignment of StMTHase and functional homologs. Catalytic residues are indicated with shaded triangles, while residues shown previously to be involved in substrate binding or enzyme activity are indicated with open triangles. Residues conserved among all the homologs in this alignment are shaded in red, while residues physiochemically conserved among all the homologs are outlined in blue. The following MTHase sequences were included in this alignment: *Salmonella typhimurium* (UniProt: Q8ZPF0), *Sulfolobus acidocaldarius* (UniProt: Q53641), *Sulfolobus solfataricus* KM1 (UniProt: Q55088), *Arthrobacter* sp. Q36 (UniProt: Q44316), and *Deinococcus radiodurans* (UniProt: Q9RX51). This alignment was created using Clustal Omega and colored using ESPript 3.0.[31,32]

The sequence and structure analysis also revealed that StMTHase contains a trehalose binding site mostly conserved with the *D. radiodurans* MTHase (DrMTHase) (Fig. 9 and 10). The +2 sub-site (see Fig. 1 for a review of sub-site nomenclature) is the most important for MTHase substrate recognition because a maltooligosaccharide and a maltooligotrehaloside only differ in the orientation of this terminal glucose monomer. Thus, researchers have crystallized DrMTHase in complex with trehalose.[15]

As previously mentioned, StMTHase contains the three catalytic residues that are characteristic of GH13 enzymes (D261, E296, and D393). It also contains residues shown in the DrMTHase to interact with the glucose monomer in the +2 sub-site. In DrMTHase, Y345 forms hydrophobic stacking interactions with this glucose monomer, while E376 hydrogen bonds with it. These residues are conserved in StMTHase, corresponding to Y339 and E371. The following residues of DrMTHase also stabilize this glucose through contacts with water molecules: D328, D329, and R380. These residues are conserved in StMTHase and correspond to D322, D323, and R373, respectively (Fig. 9 and 10).[15]

There are some residues in the trehalose binding site of DrMTHase, however, that are not conserved in StMTHase. In DrMTHase, H310 forms hydrophobic stacking interactions with the glucose monomer in the +2 sub-site. This residue is not conserved in StMTHase, corresponding to S298. The residue H332 of DrMTHase recognizes the α-1,1-glycosidic linkage of the substrate by hydrogen bonding with the O6 atom of the glucose rings in the +2 and +1 sub-sites. This residue corresponds to N326 of StMTHase. Finally, Y349 of DrMTHase helps stabilize the +2 sub-site glucose through contacts with water molecules but is not conserved in StMTHase, corresponding to F343 (Fig. 9 and 10).[15] This phenylalanine residue, however, is conserved in other functional homologs, as shown in the multi-sequence alignment (Fig. 9).

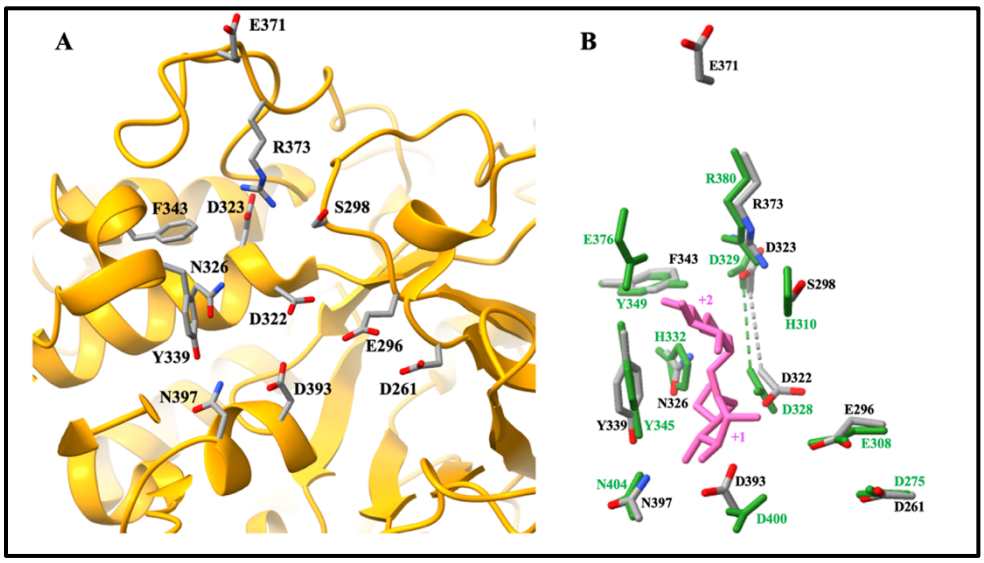

Fig. 10. Trehalose binding site of StMTHase (UniProt: Q8ZPF0, PDB: 3M07). (A) The backbone of StMTHase is shown in orange. Residues involved in binding the trehalose moiety of maltooligosyl trehalose substrates and the three conserved catalytic residues (D261, E296, and D393) are shown, colored by element, and labeled. (B) The trehalose binding site of StMTHase is overlayed with that of the *Deinococcus radiodurans* MTHase (PDB: 2BHY).[15] The side chains of StMTHase residues are colored by element and labeled in black. The side chains of *D. radiodurans* MTHase residues are colored and labeled green. The trehalose ligand is shown in pink, with the +1 and +2 sub-sites labeled. These illustrations were produced using UCSF ChimeraX.[19,20]

Structural analysis of StMTHase also revealed that it contains a maltose binding site that is conserved with that of DrMTHase. Because maltose mimics the maltooligosaccharide portion of a maltooligotrehaloside, researchers have crystallized the structure of DrMTHase in complex with maltose to reveal the -2 and -3 sub-sites (see Fig. 1).[15] To accomplish maltose binding, it was previously shown that an α-helix in DrMTHase undergoes a conformational change to trap the molecule. This α-helix is conserved in StMTHase and comprises residues H448-A467 (Fig. 11A). In DrMTHase, the residues R468 and E471 hydrogen bond with maltose. These residues correspond to R459 and E462 of StMTHase, respectively. The residues F452 and W241 of DrMTHase form hydrophobic stacking interactions with maltose and are conserved in StMTHase, corresponding to F443 and W227, respectively (Fig. 9 and 11).[15] Overall, the

substrate binding site of StMTHase, which encompasses the trehalose and maltose-binding residues, has a largely negative electrostatic surface potential. This is consistent with the DrMTHase binding site (Fig. 12).

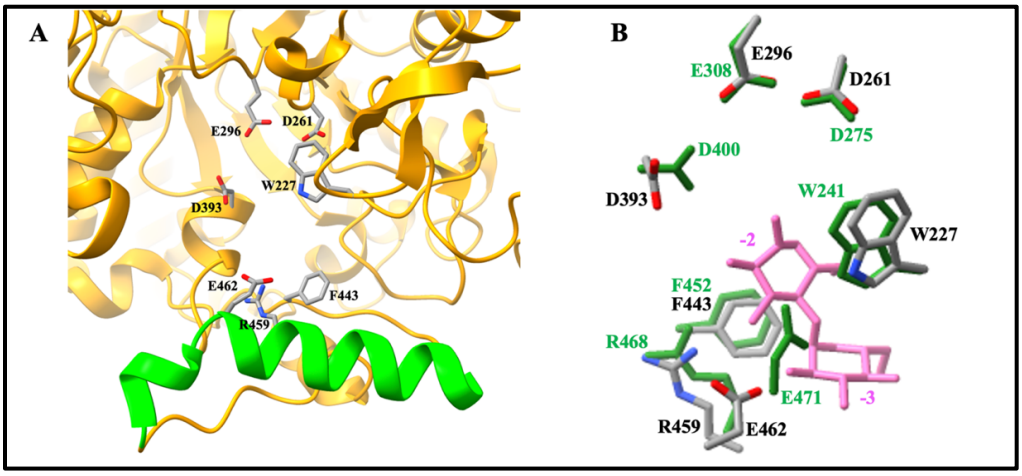

Fig. 11. Maltose binding site of StMTHase (UniProt: Q8ZPF0, PDB: 3M07). (A) The backbone of StMTHase is shown in orange. Residues involved in binding maltose and the three conserved catalytic residues (D261, E296, and D393) are shown, colored by element, and labeled. A conserved α-helix shown to undergo a conformational change in the *Deinococcus radiodurans* MTHase to trap maltose in the channel leading to the active site is shown in green. (B) The maltose binding site of StMTHase is overlayed with that of the *D. radiodurans* MTHase (PDB: 2BHZ).[15] The side chains of StMTHase residues are colored by element and labeled in black. The side chains of *D. radiodurans* MTHase residues are colored and labeled green. The maltose ligand is shown in pink, with the -2 and -3 sub-sites labeled. These illustrations were produced using UCSF ChimeraX.[19,20]

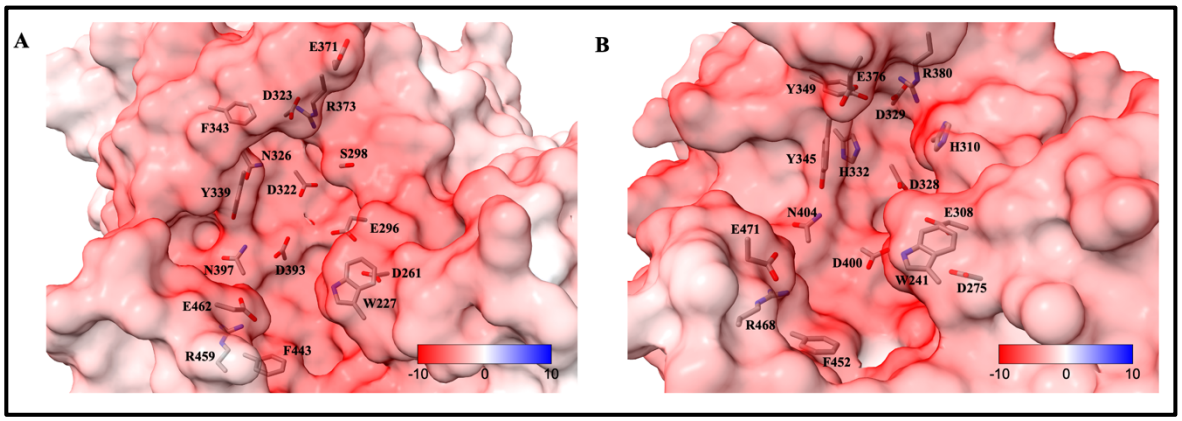

Fig. 12. Electrostatic surface potential of StMTHase (UniProt: Q8ZPF0, PDB: 3M07). The electrostatic surface potentials of (A) the StMTHase binding site and (B) the binding site of the MTHase from *Deinococcus radiodurans* (UniProt: Q9RX51, PDB: 2BHU) are shown.[15] The side chains of binding site amino acids are shown and colored by element. Regions of negative electrostatic potential are shown in red, whereas regions of positive electrostatic potential are shown in blue. The electrostatic surface potential of each protein was calculated using the Adaptive Poisson Boltzmann Solver (APBS) web server.[33] These illustrations were produced using UCSF ChimeraX.[19,20]

The overall domain architecture of StMTHase is shown in Fig. 13. The enzyme consists of three major domains. Domain A (A113-S524) is the catalytic domain and contains a $(\beta/\alpha)_8$-barrel structure. There are two insertions into the $(\beta/\alpha)_8$-barrel, referred to as subdomains B (V200-V235) and D (E434-G495). Domain E (M1-Q112) is located at the N-terminus, while domain C (G525-S594) is located at the C-terminus. The active site is formed by domain A and its subdomains. The conserved catalytic amino acids (D261, E296, and D393) are located at the center of the $(\beta/\alpha)_8$-barrel. This overall structure is like the MTHases from *S. solfataricus* KM1 and *D. radiodurans*. However, the *S. solfataricus* KM1 MTHase is a symmetric homodimer, with the monomers joined by an intermolecular disulfide bond.[10,15] The cysteine residue involved in dimerization is not conserved in StMTHase (corresponding to N312) or in the other non-archaea MTHases included in the alignment (Fig. 9).

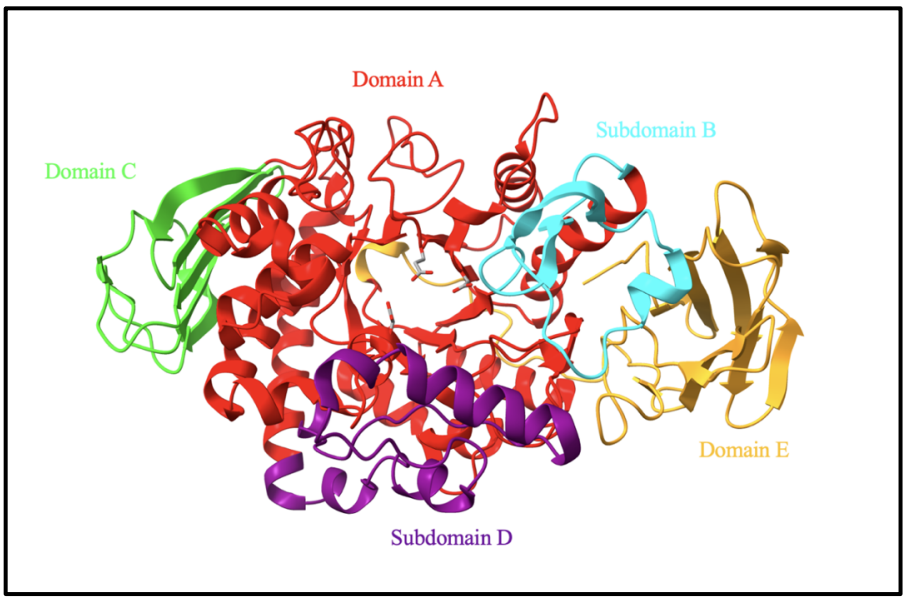

Fig. 13. Domain architecture of StMTHase (UniProt: Q8ZPF0, PDB: 3M07). The major domains and subdomains of domain A are individually colored and labeled. The side chains of the three conserved catalytic residues (D261, E296, and D393) are shown and colored by element at the center of the $(\beta/\alpha)_8$-barrel of domain A. This illustration was produced using UCSF ChimeraX.[19,20]

Production of Mutant StMTSases Using Site-Directed Mutagenesis

Computational analysis revealed that a tyrosine cluster present in several functional MTSases and which forms part of the +1 sub-site is only partially conserved in StMTSase. Specifically, StMTSase contains two residues (M460 and V464) which correspond to tyrosine residues in other homologs (Fig. 5 and 6). Thus, we sought to investigate whether these amino acids are important for StMTSase function.

Site-directed mutagenesis was used to generate a plasmid encoding a mutant StMTSase containing two substitutions (M460Y and V464Y). PCR was performed using the pMcSGJ3 plasmid, which was provided by the CSGID and encodes the wild-type StMTSase as the template, and the primers SDM1F and SDM1R to generate the M460Y and V464Y mutations (primer and plasmid information are provided in Tables A1 and A3). The 60 μL PCR was

equally divided into six separate PCR tubes, each of which experienced a different annealing temperature to determine the optimal primer annealing temperature. Agarose gel electrophoresis was conducted to confirm the presence of PCR products. As shown in Fig. 14, annealing temperatures of 58.3°C, 61.4°C, and 72°C successfully yielded PCR products. This plasmid was named "pMcSGJ3-M460Y-V464Y". It was transformed into competent DH5α *E. coli* cells for replication. Once replicated, the plasmid was isolated from the cells, and a sample was sent to Eurofins Genomics for sequencing. As shown in Table A4, pMcSGJ3-M460Y-V464Y contains the M460Y and V464Y mutations.

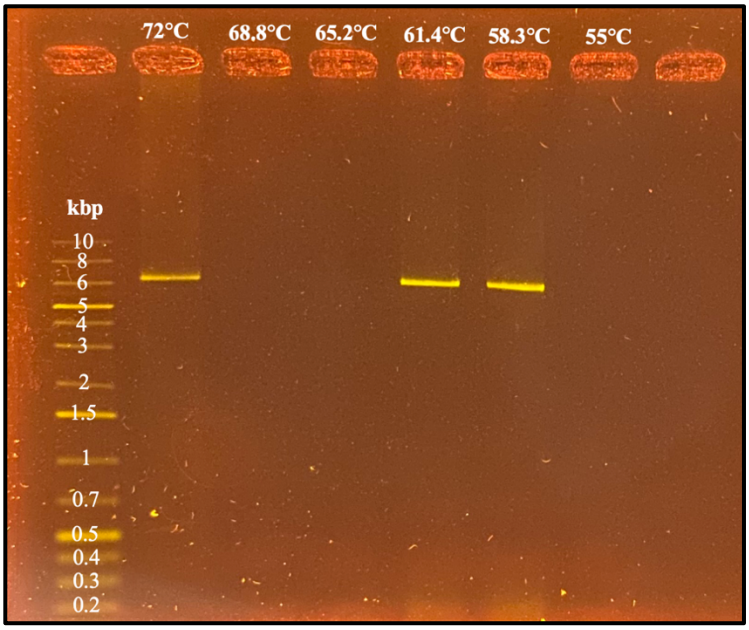

Fig. 14. Agarose gel of the PCR used to generate pMcSGJ3-M460Y-V464Y. The pMcSGJ3 plasmid was used as the template, and the primers SDM1F and SDM1R were used to generate the M460Y and V464Y mutations. The annealing temperatures used are shown at the top of the gel. Annealing temperatures of 72°C, 61.4°C, and 58.3°C yielded PCR products. The GeneRuler 1 kb Plus DNA ladder is shown in the leftmost lane.

Site-directed mutagenesis was also used to generate a plasmid encoding a mutant StMTSase containing one substitution (M460Y). PCR was performed using the pMcSGJ3

plasmid as the template and the primers SDM2F and SDM2R to generate the M460Y mutation (primer and plasmid information are provided in Tables A1 and A3). The 50 μL PCR was equally divided into five separate PCR tubes, each of which experienced a different annealing temperature to determine the optimal primer annealing temperature. Agarose gel electrophoresis was conducted to confirm the presence of PCR products. Figure 15 shows that 55°C and 40°C annealing temperatures yielded PCR products, although the DNA bands were very faint. The contents of the fifth PCR tube (annealing temperature of 51.9°C) evaporated in the thermocycler. Thus, only four samples were loaded into the gel. This plasmid was named "pMcSGJ3-M460Y". It was transformed into competent DH5α *E. coli* cells for replication. Once replicated, the plasmid was isolated from the cells, and a sample was sent to Eurofins Genomics for sequencing. As shown in Table A4, pMcSGJ3-M460Y contains the M460Y mutation. Our laboratory is currently working to produce an additional mutant (StMTSase-V464Y). However, the production of this mutant was delayed due to problems with mutagenesis.

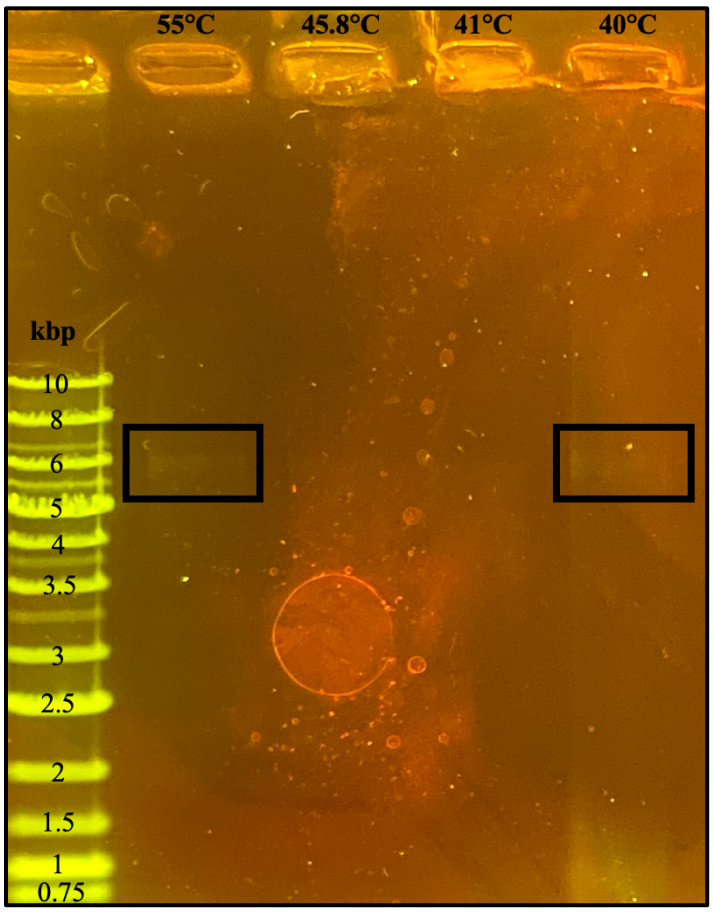

Fig. 15. Agarose gel of the PCR used to generate pMcSGJ3-M460Y. The pMcSGJ3 plasmid was used as the template, and the primers SDM2F and SDM2R were used to generate the M460Y mutation. The annealing temperatures used are shown at the top of the gel. Annealing temperatures of 55°C and 40°C yielded faint PCR products (boxed in black). The GeneRuler 1 kb DNA ladder is shown in the leftmost lane.

Overexpression and Purification of StMTSases

The Center for Structural Genomics of Infectious Diseases (CSGID) provided the pMcSGJ3 plasmid, which encodes wild-type StMTSase in fusion with a polyhistidine tag. This plasmid and the pMcSGJ3-M460Y-V464Y and pMcSGJ3-M460Y plasmids produced by our laboratory were separately transformed into BL21 *E. coli* cells. Wild-type StMTSase, StMTSase-M460Y-V464Y, and StMTSase-M460Y were then overexpressed in BL21 *E. coli* using a final concentration of 1 mM Isopropyl β-D-1-thiogalactopyranoside (IPTG), which triggered

transcription of the *lactose* operon. Once overexpressed, the enzymes were purified from the cells using immobilized metal affinity chromatography (IMAC). The protein content of the final protein stocks was analyzed using sodium dodecyl sulfate-polyacrylamide gel electrophoresis (SDS-PAGE). Figures 16 and 17 show that the wild-type and mutant StMTSase stocks used in this study were pure, each containing a single protein of the expected size (95 kDa), as indicated by the presence of a single band.

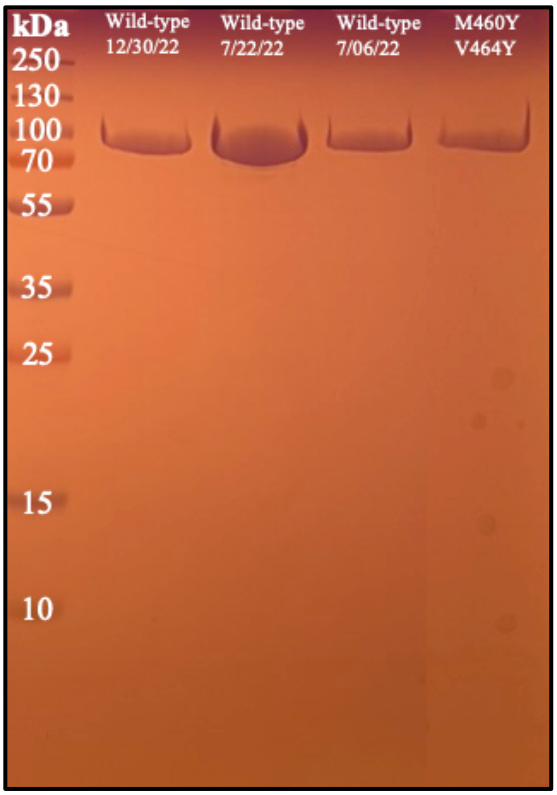

Fig. 16. SDS-PAGE results for purification of StMTSase and StMTSase-M460Y-V464Y. The content of the protein stocks used throughout this study is shown. The protein stocks each contained a single protein of the expected size (95 kDa). The PageRuler Plus protein ladder is shown in the leftmost lane of the gel.

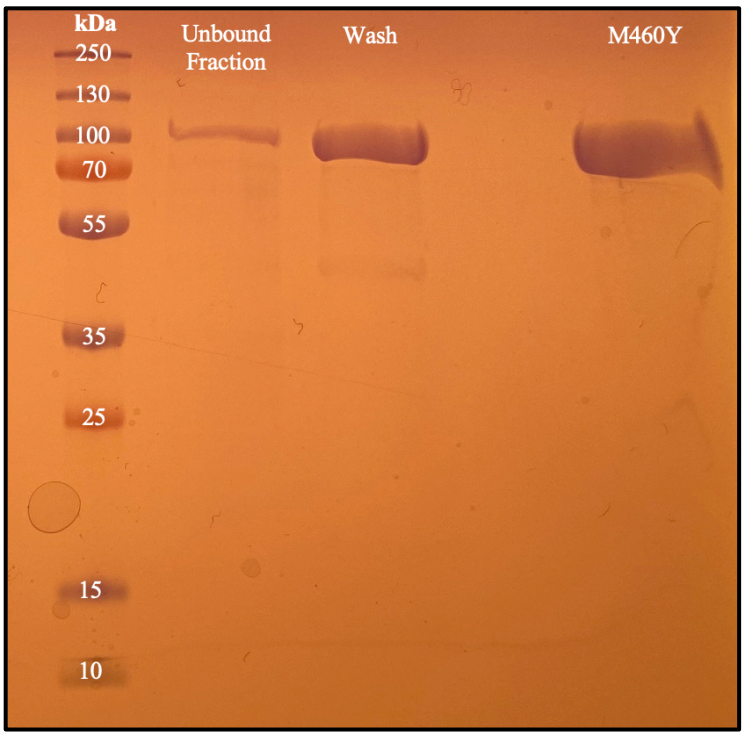

Fig. 17. SDS-PAGE results for purification of StMTSase-M460Y. The protein content of the unbound fraction, wash flow-through, and final StMTSase-M460Y protein stock is shown. The protein stock contained a single protein of the expected size (95 kDa). The PageRuler Plus protein ladder is shown in the leftmost lane of the gel.

Determination of StMTSase Concentration

The concentrations of the wild-type and mutant StMTSase stocks used for the enzyme activity assays performed in this study were determined using a Bradford assay. Bovine serum albumin (BSA) standards ranging from 0-0.25 mg/mL were prepared by serial dilution. At the same time, serial dilutions were made of the wild-type and mutant StMTSase stocks. The BSA standards and dilutions of the protein stocks were mixed with Coomassie Plus Reagent in duplicate, and their absorbances (595 nm) were measured using a microplate spectrophotometer. The concentrations of the protein stocks were determined using a BSA standard curve. The calculated concentrations are displayed in Table 5.

Table 5. Concentrations of the protein stocks used throughout this study. Serial dilutions of the protein stocks used throughout this study were prepared and mixed with Coomassie Plus Reagent in duplicate. Their absorbances (595 nm) were measured using a microplate spectrophotometer. Their concentrations were calculated from a BSA standard curve.

Protein Stock	**Concentration (mg/mL)**
Wild-type 7.06.22	0.80
Wild-type 7.22.22	3.09
Wild-type 12.30.22	0.78
StMTSase-M460Y-V464Y	0.63
StMTSase-M460Y	1.02

StMTSase Activity on Various Substrates

The Nelson-Somogyi (NS) method, a colorimetric method of detecting reducing sugars, was used to monitor StMTSase activity. This is because MTSase enzymes convert reducing maltooligosaccharides into the nonreducing saccharide maltooligosyl trehalose.[30] StMTSase activity was surveyed for three substrates. StMTSase utilized maltohexaose and dextrin as substrates, but not maltotriose. Maltohexaose, rather than dextrin, was used as the substrate for all further enzyme activity assays because it is a single compound for which a molecular weight exists. Dextrin is a mixture of glucose polymers, some of which will serve as a substrate for the enzyme, while others will not.

Temperature-Dependence of StMTSase

To determine the temperature optimum of StMTSase, enzymatic reactions were performed at temperatures ranging from 7°C-57°C and consisted of purified StMTSase and pH 7.0 maltohexaose substrate. The reactions proceeded for 45 min and were stopped using a boiling water bath. Control reactions went immediately into a boiling water bath upon adding StMTSase. The Nelson-Somogyi (NS) method was used to monitor StMTSase activity.[30] Relative enzyme activity was assessed based on the decreased absorbances (600 nm) observed for the enzymatic

reactions compared to the controls. As shown in Fig. 18, StMTSase functioned optimally at 40°C.

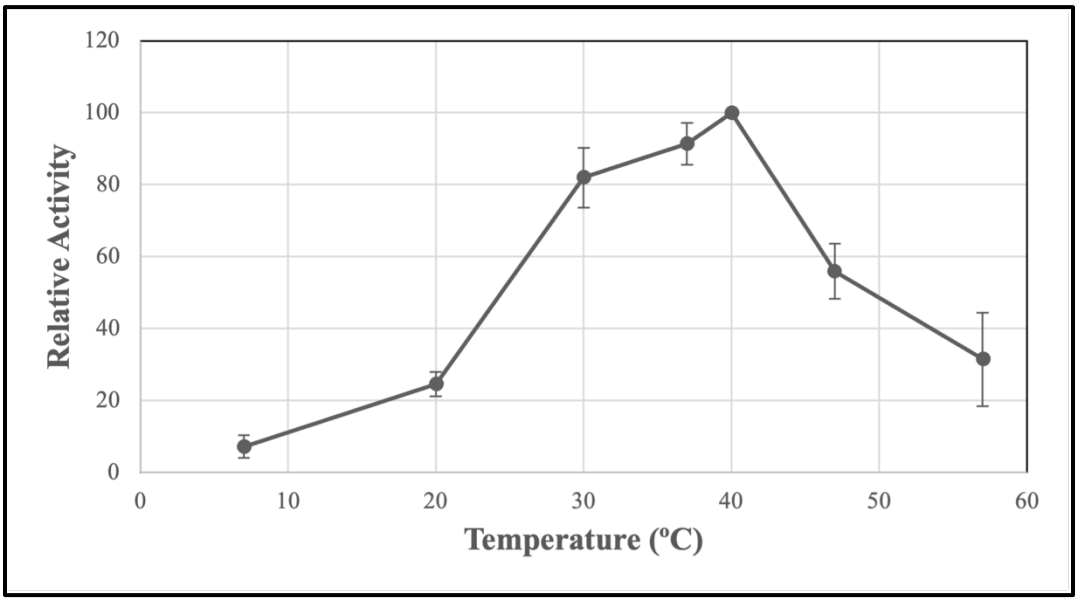

Fig. 18. StMTSase functions optimally at 40°C. Maltohexaose was used as the substrate. Reactions proceeded for 45 min at temperatures controlled using water baths and at a pH of 7.0. The reactions were stopped using a boiling water bath, while control reactions went immediately into a boiling water bath upon receiving the enzyme. Relative StMTSase activity was determined using the Nelson-Somogyi (NS) method for the detection of reducing sugars.[30] This experiment was performed in triplicate, the average of which is shown. Error bars represent the standard deviation.

pH-Dependence of StMTSase

To determine the pH optimum of StMTSase, enzymatic reactions were performed at pHs ranging from 4.0-10.94 and consisted of purified StMTSase and maltohexaose substrate in an appropriate buffer. The reactions proceeded for 45 min at 40°C and were stopped using a boiling water bath. Control reactions went immediately into a boiling water bath upon adding StMTSase. The Nelson-Somogyi (NS) method was used to monitor StMTSase activity.[30] Relative enzyme activity was assessed based on the decreased absorbances (600 nm) observed for the enzymatic

reactions compared to the controls. As shown in Fig. 19, StMTSase functioned optimally at a pH of 7.0.

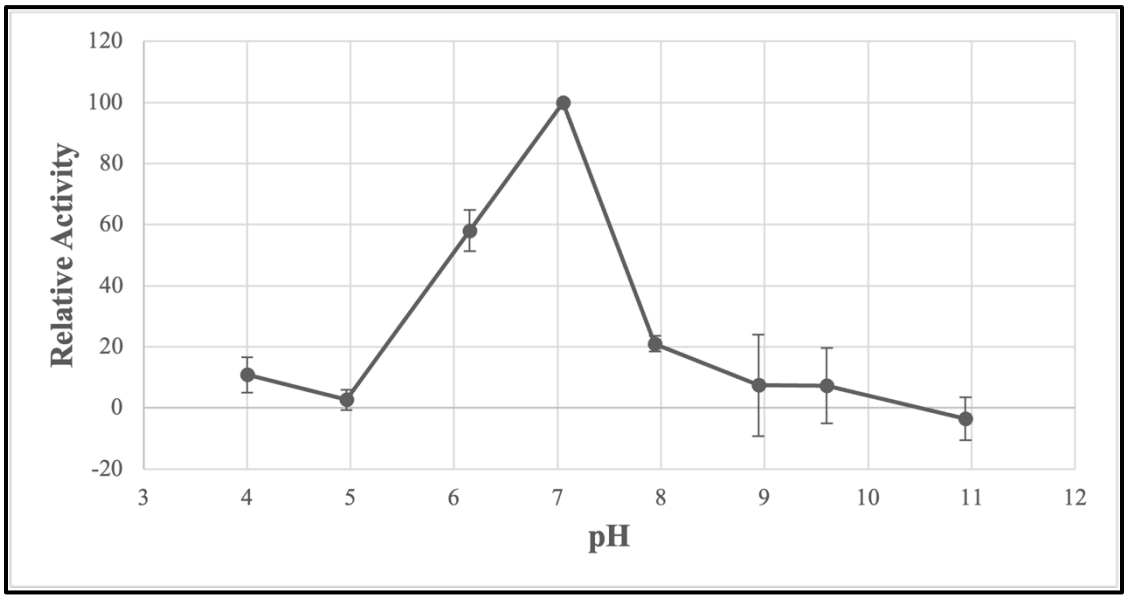

Fig. 19. StMTSase functions optimally at a pH of 7.0. Maltohexaose was used as the substrate. Reactions proceeded for 45 min at 40°C. pHs were controlled using buffers, and the reactions were stopped using a boiling water bath. Control reactions went immediately into a boiling water bath upon receiving the enzyme. Relative StMTSase activity was determined using the Nelson-Somogyi (NS) method for the detection of reducing sugars.[30] This experiment was performed in triplicate, the average of which is shown. Error bars represent the standard deviation.

Effects of Potassium and Bovine Serum Albumin on StMTSase Activity

To identify potential activators of StMTSase, the effects of potassium and bovine serum albumin (BSA) on the enzyme's activity were evaluated. All enzymatic reactions consisted of purified StMTSase and maltohexaose substrate in pH 7.0 McIlvaine buffer. Some reactions also contained 300 mM KCl, 0.6 mg/mL BSA, or both. All reactions proceeded for 45 min at 40°C and were stopped using a boiling water bath. Control reactions went immediately into a boiling water bath upon adding StMTSase. The Nelson-Somogyi (NS) method was used to monitor

StMTSase activity.[30] Enzyme activity was assessed based on the decreased absorbances of the enzymatic reactions compared to the controls with units of ΔAbs mg^{-1} min^{-1}.

As shown in Fig. 20, adding 300 mM KCl significantly increased StMTSase activity compared to pH 7.0 McIlvaine buffer alone ($p = 0.003$). No further increase in StMTSase activity was achieved by adding greater than 300 mM KCl to the reaction buffer (data not shown). In contrast, adding 0.6 mg/mL BSA, which is often added to enzymatic reactions and storage buffers to stabilize enzymes and prevent them from adhering to plastic surfaces, significantly decreased StMTSase activity compared to pH 7.0 McIlvaine buffer alone ($p = 0.03$).

Follow-up experiments showed that supplementing the reaction buffer with NaCl had no effect on StMTSase activity, whereas the enzyme's activity decreased when the reaction buffer was supplemented with $MgCl_2$ (data not shown). Adding glycerol or dithiothreitol (DTT) to the reaction buffer interfered with the NS assay, produced a dark black color, and prevented enzyme activity data from being obtained.

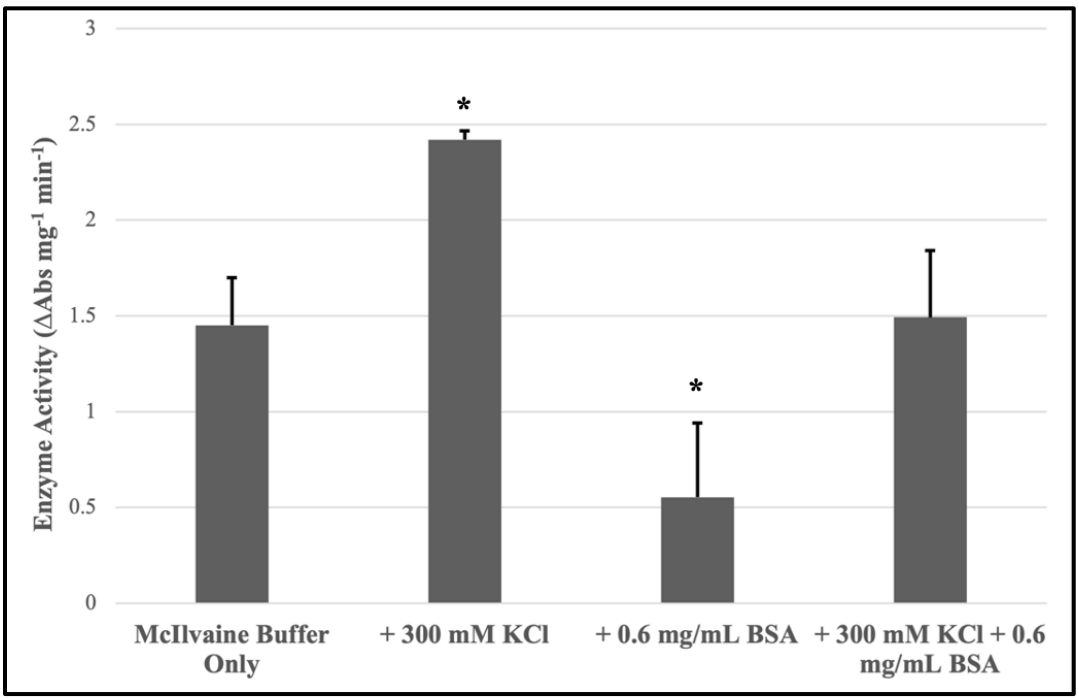

Fig. 20. Potassium increases StMTSase activity, while BSA decreases StMTSase activity. All reactions contained maltohexaose and purified StMTSase in pH 7.0 McIlvaine buffer; some contained 300 mM KCl, 0.6 mg/mL BSA, or both. All reactions proceeded for 45 min at 40°C and were stopped using a boiling water bath. Control reactions went immediately into a boiling water bath upon receiving the enzyme. StMTSase activity was evaluated using the Nelson-Somogyi (NS) method of detecting reducing sugars with units of ΔAbs mg^{-1} min^{-1}.[30] This experiment was performed in triplicate, the average of which is shown. Error bars represent the standard deviation. Asterisks indicate a significant difference, as determined by an unpaired student t-test, from the activity of StMTSase in pH 7.0 McIlvaine buffer only (α=0.05).

Effect of Maltohexaose Concentration on the Reaction Rate

This study assessed StMTSase activity across increasing maltohexaose concentrations with the goal of obtaining a Michaelis-Menten saturation curve. Obtaining this curve would allow for determining some of this enzyme's basic kinetic properties, including the maximal reaction rate (V_{max}) and the Michaelis constant (K_m). The Michaelis constant is the substrate concentration at which the reaction rate is half of the maximal rate and is often used to assess an enzyme's affinity for a substrate. Lower K_m values indicate a higher affinity for a substrate, whereas higher K_m values indicate a lower affinity.

To do this, maltohexaose in pH 7.0 McIlvaine buffer containing 300 mM KCl was used as the substrate. A range of substrate concentrations was obtained via serial dilution. Enzymatic reactions and controls consisted of the substrate and purified StMTSase. The enzymatic reactions proceeded for 45 min at 40°C and were stopped using a boiling water bath. Control reactions went immediately into a boiling water bath upon adding the enzyme. Reducing sugars were then quantified using the Nelson-Somogyi method, as described previously.[30] A maltohexaose standard curve was produced using the absorbance values of the controls. This standard curve was used to determine the change in maltohexaose concentration between each enzymatic reaction and the corresponding control. The reaction rate was calculated with units of mmol mg^{-1} min^{-1}. As shown in Fig. 21, a saturation curve was not obtained. Rather, the StMTSase reaction rate increased linearly as the maltohexaose concentration increased to 18 mM. Further increasing the maltohexaose concentration to above 50 mM produced similar results (data not shown), while also consuming large amounts of the substrate and other resources. Thus, replicates of this were not performed. Significantly higher maltohexaose concentrations might be needed to reach the maximal reaction rate for StMTSase. Otherwise, the reaction or storage conditions may not be quite optimal, preventing the enzyme from functioning maximally.

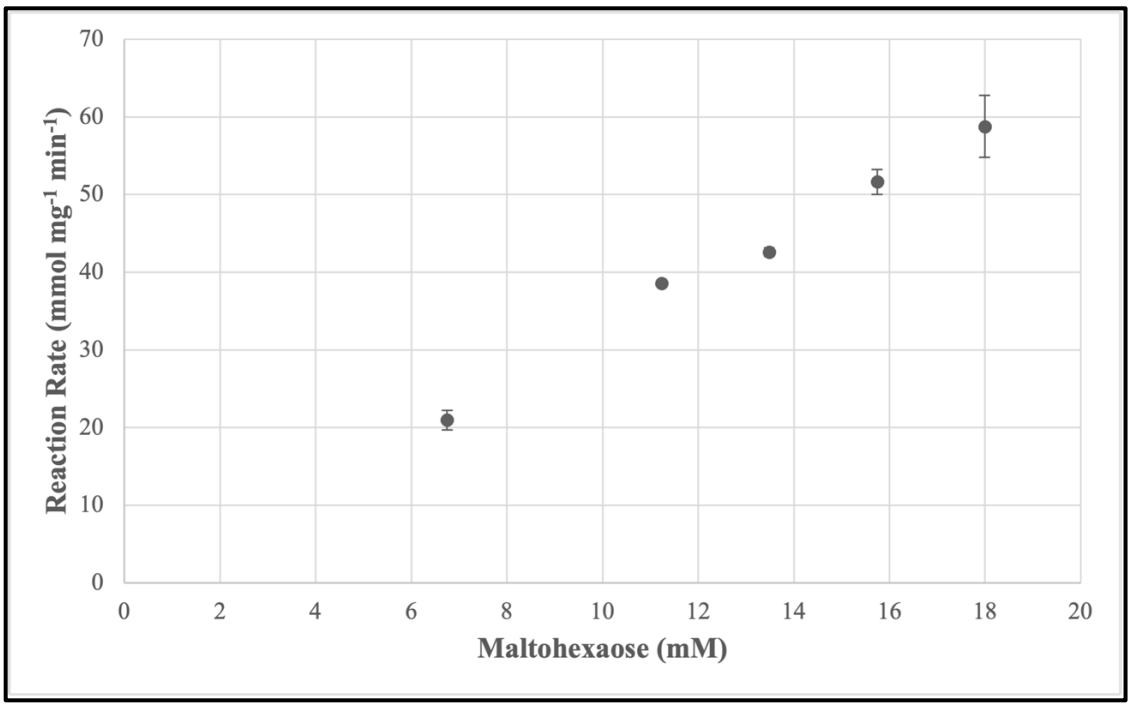

Fig. 21. The StMTSase reaction rate increases linearly as the maltohexaose concentration increases to 18 mM. Maltohexaose in pH 7.0 McIlvaine buffer containing 300 mM KCl was used as the substrate. A range of substrate concentrations was obtained via serial dilution. The enzymatic reactions proceeded for 45 min at 40°C and were stopped using a boiling water bath, while controls went immediately into a boiling water bath upon adding the enzyme. Reducing sugars were quantified using the Nelson-Somogyi (NS) method.[30] A maltohexaose standard curve was produced using the absorbance values of the controls and was used to calculate the reaction rates with units of mmol mg^{-1} min^{-1}. This experiment was performed in duplicate, the average of which is shown. Error bars represent the standard deviation.

Activity of Mutant StMTSases

As previously mentioned, a tyrosine cluster contributing to the +1 sub-site in the MTSase from *S. acidocaldarius* (SaMTSase) and conserved in several other functional homologs is only partially conserved in StMTSase. Specifically, Y388 and Y392 of SaMTSase correspond to M460 and V464 of StMTSase (Fig. 5 and 6B). Y392 of SaMTSase is proposed to hydrogen bond with the glucose monomer in the +1 sub-site following its 180° rotation to convert the α-1,4-glycosidic linkage to an α-1,1-glycosidic linkage. Thus, we were interested in whether substituting M460 and V464 of StMTSase with tyrosine would impact the enzyme's activity.

Site-directed mutagenesis was used to generate two mutant StMTSases: StMTSase-M460Y-V464Y and StMTSase-M460Y. The activity of each of these mutants, alongside the wild-type enzyme, was assessed. Maltohexaose in pH 7.0 McIlvaine buffer containing 300 mM KCl was used as the substrate. Enzymatic reactions were performed at 40°C for 45 min and were stopped using a boiling water bath. Control reactions went immediately into a boiling water bath upon adding the enzyme. Enzyme activity was assessed based on the decreased absorbances of the enzymatic reactions compared to the controls with units of ΔAbs mg^{-1} min^{-1}. As shown in Fig. 22, enzyme activity was not detected for StMTSase-M460Y-V464Y. In contrast, no significant difference was found between the activity of wild-type StMTSase and StMTSase-M460Y ($p = 0.055$).

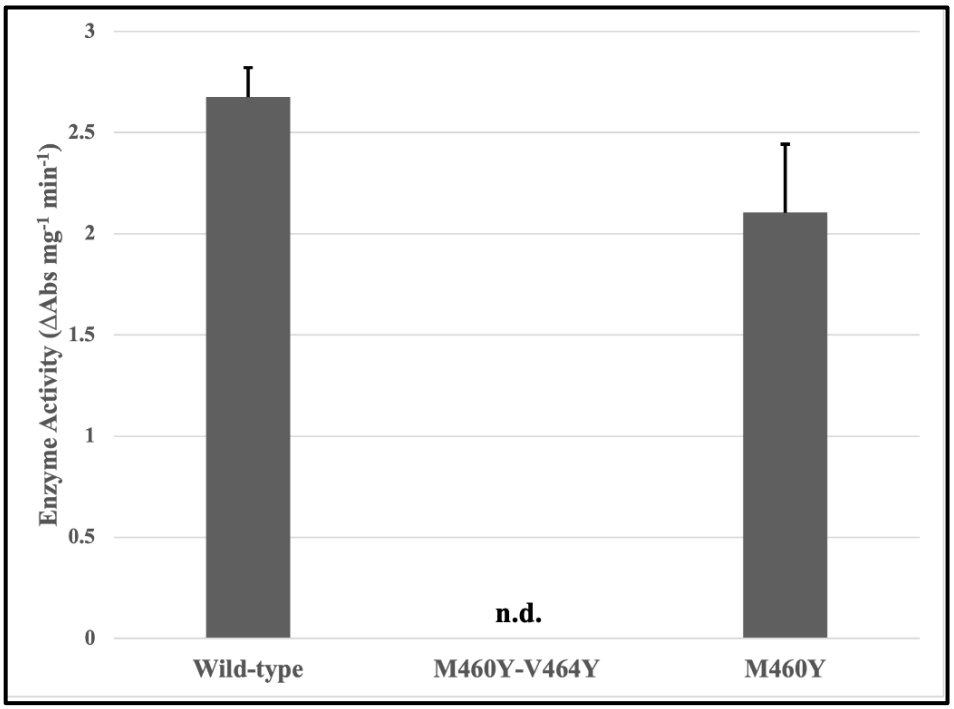

Fig. 22. StMTSase-M460Y-V464Y is nonfunctional, whereas StMTSase-M460Y displays activity comparable to wild-type StMTSase. Maltohexaose in pH 7.0 McIlvaine buffer containing 300 mM KCl was used as the substrate. Enzymatic reactions proceeded for 45 min at 40°C and were stopped using a boiling water bath. Control reactions went immediately into a boiling water bath upon receiving the enzyme. StMTSase activity was evaluated using the

Nelson-Somogyi (NS) method of detecting reducing sugars with units of ΔAbs mg^{-1} min^{-1}.[30] This experiment was performed in triplicate, the average of which is shown. Error bars represent the standard deviation. No significant difference was found between the activity of wild-type StMTSase and StMTSase-M460Y, as determined by an unpaired student t-test (α=0.05). n.d.: not detectable

CHAPTER FOUR: DISCUSSION

This study sought to characterize a putative trehalose biosynthetic pathway in *Salmonella typhimurium*, comprised of two enzymes: maltooligosyl trehalose synthase (StMTSase) and maltooligosyl trehalose trehalohydrolase (StMTHase). To accomplish this, several approaches were taken. First, computational analysis of both enzymes was performed to compare their sequences and structures to functional homologs. This allowed for identifying conserved features, which support function, and differences in sequence and structure. Second, several enzymatic properties of the StMTSase were biochemically characterized. These include its activity towards different substrates, temperature and pH optima, activity in the presence of potential activators, and activity in response to increasing maltohexaose concentration. Third, two mutant StMTSases were produced to assess the importance of two amino acids for enzyme function (M460 and V464). These amino acids reside in the substrate binding site and are non-conserved with the tyrosine residues present in some other functional homologs.[17]

The computational analysis of StMTSase revealed that all three amino acids known in the literature to be catalytic (D251, E279, and D517) are conserved in its sequence and structure.[17] This enzyme contains most amino acids known to participate in substrate binding or that have been shown previously by mutational analysis to be important for MTSase function (Fig. 5 and 6) and has an electrostatic surface potential that is consistent with functional homologs (Fig. 7).[7,17] StMTSase has a domain architecture like that of functional homologs, containing a catalytic $(\beta/\alpha)_8$-barrel structure at its core, which is a characteristic of α-amylase family enzymes (Fig. 8).[7,9,17] Altogether, these results are suggestive of a functional enzyme.

Like the StMTSase, the computational analysis of the StMTHase revealed that this enzyme contains all three catalytic amino acids reported in the literature (D261, E296, and D393) (Fig. 9).[10] StMTHase retains largely conserved trehalose and maltose binding sites (Fig. 10-11) and has an electrostatic surface potential that is consistent with functional homologs (Fig. 12). This enzyme also contains a catalytic $(\beta/\alpha)_8$-barrel structure at its core and is similar in overall architecture to functional homologs (Fig. 13).[10,15] In total, these results suggest that StMTHase is also a functional enzyme.

The biochemical characterization of the StMTSase revealed several of its enzymatic properties. This enzyme was catalytically active on maltohexaose and dextrin, but activity was not detected when maltotriose was used as the substrate. These results are consistent with the literature as the MTSase from *Arthrobacter* sp. Q36 shows a greater affinity for longer maltooligosaccharides, with minimal activity observed for maltotriose.[13] Maltohexaose, rather than dextrin, was used as the substrate for all further enzyme activity assays because it is a single compound for which a molecular weight exists. Dextrin is a mixture of glucose polymers, some of which will serve as a substrate for the enzyme, while others will not.

StMTSase functioned optimally at 40°C and a pH of 7.0 (Fig. 18 and 19). These results are consistent with the temperature and pH optima reported for the MTSase from *Arthrobacter* sp. Q36, a Gram-positive bacterial species commonly found in soil.[13] As expected, however, this enzyme's temperature and pH optima are different from that of MTSases in the archaeal extremophiles *Sulfolobus acidocaldarius* and *Sulfolobus tokodaii*, which are reported to function optimally at 75°C and a pH of 5.0.[4,6] Interestingly, Kobayashi et al. reported two salt bridges that may be related to thermostability in their structural characterization of the MTSase from *S. acidocaldarius*: D54/R99 and E212/R99.[17] This arginine residue (R99) is not conserved in either

MTSase from *Arthrobacter* sp. Q36 or StMTSase, having been replaced by tryptophan in both enzymes. This could contribute to their reduced temperature optima.

StMTSase was also found to function best in the presence of potassium. Including 300 mM KCl in the reaction buffer resulted in a significant increase in StMTSase activity compared to without (Fig. 20). This was not entirely surprising, as potassium is the most abundant cation in bacterial cells, with concentrations generally maintained between 300 mM and 500 mM, where it is often an activator of cytoplasmic enzymes.[36] However, potassium is not reported to have been included in any of the sodium phosphate or citrate phosphate (McIlvaine) buffers used to characterize MTSase enzymes previously.[4,6,13] This could be a unique difference in the activity of StMTSase compared to the known functional homologs. Additionally, the presence of bovine serum albumin (BSA) in the reaction buffer significantly decreased StMTSase activity (Fig. 20). This result was surprising as BSA is often added to reaction and storage buffers to stabilize enzymes and prevent them from adhering to the surfaces of tubes and pipette tips. Follow-up experiments showed that supplementing the reaction buffer with NaCl did not affect StMTSase activity, whereas supplementing the reaction buffer with $MgCl_2$ decreased the enzyme's activity (data not shown). This is consistent with the literature as MTSase enzymes have been shown to be inhibited by divalent cations.[13] Adding glycerol or dithiothreitol (DTT) to the reaction buffer interfered with the NS assay, produced a dark black color, and prevented activity data from being obtained.

StMTSase activity was also evaluated across increasing maltohexaose concentrations, with the goal of obtaining its basic kinetic properties. These include the maximal reaction rate (V_{max}) and the Michaelis constant (K_m). The K_m is the substrate concentration at which the reaction rate is half of the maximal rate and is often used as a measure of substrate affinity.

Generally, a lower K_m indicates a higher affinity for a substrate, whereas a higher K_m often indicates a lower affinity. A linear relationship was observed between the StMTSase reaction rate and increasing maltohexaose concentration (rather than the expected hyperbolic relationship) (Fig. 21). This result was unexpected, as the StMTSase reaction rate showed no signs of slowing down even at maltohexaose concentrations well above the reported K_m values for functional homologs. For example, the MTSase from *Arthrobacter* sp. Q36 is reported to have a K_m value of 1.4 mM for maltohexaose.[13] Significantly higher maltohexaose concentrations might be needed to reach the maximal reaction rate for StMTSase. This would suggest that the enzyme has a lower affinity for maltohexaose than the MTSase from *Arthrobacter* sp. Q36 or that a different substrate is preferred.[13] Alternatively, the reaction or storage conditions may not be quite optimal, preventing the enzyme from functioning maximally. One could explore how adding stabilizers (such as glycerol, polyethylene glycol (PEG), or BSA) to the storage buffer affects the enzyme's activity and whether its activity is significantly affected by freeze-thaw cycles. It would also be worth exploring whether StMTSase activity is activated by the presence of the StMTHase. Perhaps these enzymes must physically interact to approach a maximal reaction rate.

Finally, we were interested in whether substituting tyrosine for M460 and V464 of StMTSase would impact the enzyme's activity as these residues reside in the substrate binding site and are non-conserved with most other homologs. Thus, two mutants were created using site-directed mutagenesis (StMTSase-M460Y-V464Y and StMTSase-M460Y) (Fig. 14 and 15). Their activities were experimentally tested, with StMTSase-M460Y-V464Y displaying no detectable activity and StMTSase-M460Y displaying activity comparable to wild-type StMTSase (Fig. 22). These results suggest that mutating M460 alone does not significantly affect the enzyme's stability or functionality, but that mutating V464 or a combination of the two might.

Perhaps incorporating multiple tyrosine residues into the active site compromises the enzyme's ability to bind the substrate, as tyrosine is a larger amino acid than methionine or valine. Alternatively, substituting these residues for tyrosine might lead to instability or protein unfolding. Assessing the activity of an additional mutant (StMTSase-V464Y) will hopefully provide some clarity. Our lab is currently working to generate this mutant.

There are several avenues of future research that should be pursued. First, this study only provides computational evidence that StMTHase is a functional enzyme. Biochemical characterization of this enzyme should be performed to conclude that it is functional, as we have shown for the StMTSase. Second, the basic kinetic properties of StMTSase, such as its V_{max} and K_m, have still not been determined, as there was difficulty approaching a maximal reaction rate. Future experiments should include measuring StMTSase activity at much higher substrate concentrations, evaluating whether the current purification and/or storage conditions negatively impact StMTSase activity, and determining whether the StMTSase is activated by the presence of the StMTHase. Ultimately, obtaining these basic kinetic properties will allow for a greater comparison of this enzyme to functional homologs.

Finally, some additional work is needed to clarify the importance of the two residues mutated in this study as StMTSase-M460Y displays activity comparable to the wild-type enzyme, yet StMTSase-M460Y-V464Y displays no detectable activity. As previously mentioned, our lab is in the process of generating and testing the activity of one additional mutant (StMTSase-V464Y). If this mutant is non-functional, this would provide evidence that V464 is important for StMTSase function. In contrast, if this mutant is functional, this would suggest that the combined mutation of M460 and V464 is detrimental to the enzyme.

Overall, this study is the first characterization of an MTSase/MTHase trehalose biosynthetic pathway in any species of Proteobacteria. Previously, this pathway had been studied predominantly in archaeal and bacterial extremophiles in pursuit of more efficient commercial trehalose production.[4,12] This study provides computational and experimental evidence that improves our understanding of the function of two genes reported to be essential in this organism.[29] Further characterization of this pathway could potentially lead to the development of novel therapeutics to combat this bacterial pathogen, which poses a significant threat to global health and food safety and is becoming increasingly antibiotic resistant.[25] Additionally, this study provides the first evidence that *S. typhimurium* can biosynthesize trehalose via at least two pathways: trehalose-6-phosphate synthase (TPS)/trehalose-6-phosphate phosphatase (TPP) and StMTSase/StMTHase.[26,27]

REFERENCES

1. Vanaporn M, Titball RW. Trehalose and bacterial virulence. Virulence. 2020;11(1):1192–1202. doi:10.1080/21505594.2020.1809326

2. Elbein AD. New insights on trehalose: a multifunctional molecule. Glycobiology. 2003;13(4):17R – 27. doi:10.1093/glycob/cwg047

3. Reina-Bueno M, Argandoña M, Nieto JJ, Hidalgo-García A, Iglesias-Guerra F, Delgado MJ, Vargas C. Role of trehalose in heat and desiccation tolerance in the soil bacterium Rhizobium etli. BMC Microbiology. 2012;12(1):207. doi:10.1186/1471-2180-12-207

4. Gueguen Y, Rolland J-L, Schroeck S, Flament D, Defretin S, Saniez M-H, Dietrich J. Characterization of the maltooligosyl trehalose synthase from the thermophilic archaeon *Sulfolobus acidocaldarius*. FEMS Microbiology Letters. 2001;194(2):201–206. doi:10.1111/j.1574-6968.2001.tb09470.x

5. Davies GJ, Wilson KS, Henrissat B. Nomenclature for sugar-binding subsites in glycosyl hydrolases. Biochemical Journal. 1997;321(2):557–559. doi:10.1042/bj3210557

6. Zhao M, Xu X, Yang S, Liu T, Liu B. Cloning, expression and characterization of the maltooligosyl trehalose synthase from the archaeon Sulfolobus tokodaii. Pak. J. Pharm. Sci. 2018:4.

7. Okazaki N, Blaber M, Kuroki R, Tamada T. Crystal structure of glycosyltrehalose synthase from *Sulfolobus shibatae* DSM5389. Acta Crystallographica Section F Structural Biology Communications. 2018;74(11):741–746. doi:10.1107/S2053230X1801453X

8. Kato M, Takehara K, Kettoku M, Kobayashi K, Shimizu T. Subsite Structure and Catalytic Mechanism of a New Glycosyltrehalose-producing Enzyme isolated from the Hyperthermophilic Archaeum, *Sulfolobus solfataricus* KM1. Bioscience, Biotechnology, and Biochemistry. 2000;64(2):319–326. doi:10.1271/bbb.64.319

9. Cielo CBC, Okazaki S, Suzuki A, Mizushima T, Masui R, Kuramitsu S, Yamane T. Structure of ST0929, a putative glycosyl transferase from *Sulfolobus tokodaii*. Acta Crystallographica Section F Structural Biology and Crystallization Communications. 2010;66(4):397–400. doi:10.1107/S1744309110006354

10. Feese MD, Kato Y, Tamada T, Kato M, Komeda T, Miura Y, Hirose M, Hondo K, Kobayashi K, Kuroki R. Crystal structure of glycosyltrehalose trehalohydrolase from the hyperthermophilic archaeum Sulfolobus solfataricus 1 1Edited by D. Rees. Journal of Molecular Biology. 2000;301(2):451–464. doi:10.1006/jmbi.2000.3977

11. Nakada T, Ikegami S, Chaen H, Kubota M, Fukuda S, Sugimoto T, Kurimoto M, Tsujisaka Y. Purification and Characterization of Thermostable Maltooligosyl Trehalose Trehalohydrolase

from the Thermoacidophilic Archaebacterium *Sulfolobus acidocaldarius*. Bioscience, Biotechnology, and Biochemistry. 1996;60(2):267–270. doi:10.1271/bbb.60.267

12. Kobayashi K, Komeda T, Miura Y, Kettoku M, Kato M. Production of trehalose from starch by novel trehalose-producing enzymes from Sulfolobus solfataricus KM1. Journal of Fermentation and Bioengineering. 1997;83(3):296–298. doi:10.1016/S0922-338X(97)80996-8

13. Nakada T, Maruta K, Tsusaki K, Kubota M, Chaen H, Sugimoto T, Kurimoto M, Tsujisaka Y. Purification and Properties of a Novel Enzyme, Maltooligosyl Trehalose Synthase, from *Arthrobacter* sp. Q36. Bioscience, Biotechnology, and Biochemistry. 1995;59(12):2210–2214. doi:10.1271/bbb.59.2210

14. Nakada T, Maruta K, Mitsuzumi H, Kubota M, Chaen H, Sugimoto T, Kurimoto M, Tsujisaka Y. Purification and Characterization of a Novel Enzyme, Maltooligosyl Trehalose Trehalohydrolase, from *Arthrobacter* sp. Q36. Bioscience, Biotechnology, and Biochemistry. 1995;59(12):2215–2218. doi:10.1271/bbb.59.2215

15. Timmins J, Leiros H-KS, Leonard G, Leiros I, McSweeney S. Crystal Structure of Maltooligosyltrehalose Trehalohydrolase from Deinococcus radiodurans in Complex with Disaccharides. Journal of Molecular Biology. 2005;347(5):949–963. doi:10.1016/j.jmb.2005.02.011

16. da Costa-Latgé SG, Bates P, Dillon R, Genta FA. Characterization of Glycoside Hydrolase Families 13 and 31 Reveals Expansion and Diversification of α-Amylase Genes in the Phlebotomine Lutzomyia longipalpis and Modulation of Sandfly Glycosidase Activities by Leishmania Infection. Frontiers in Physiology. 2021;12:635633. doi:10.3389/fphys.2021.635633

17. Kobayashi M, Kubota M, Matsuura Y. Refined Structure and Functional Implications of Trehalose Synthase from Sulfolobus acidocaldarius. Journal of Applied Glycoscience. 2003;50(1):1–8. doi:10.5458/jag.50.1

18. Wierenga RK. The TIM-barrel fold: a versatile framework for efficient enzymes. FEBS Letters. 2001;492(3):193–198. doi:10.1016/S0014-5793(01)02236-0

19. Pettersen EF, Goddard TD, Huang CC, Meng EC, Couch GS, Croll TI, Morris JH, Ferrin TE. UCSF CHIMERAX : Structure visualization for researchers, educators, and developers. Protein Science. 2021;30(1):70–82. doi:10.1002/pro.3943

20. Goddard TD, Huang CC, Meng EC, Pettersen EF, Couch GS, Morris JH, Ferrin TE. UCSF ChimeraX: Meeting modern challenges in visualization and analysis: UCSF ChimeraX Visualization System. Protein Science. 2018;27(1):14–25. doi:10.1002/pro.3235

21. dos Santos AMP, Ferrari RG, Conte-Junior CA. Virulence Factors in Salmonella Typhimurium: The Sagacity of a Bacterium. Current Microbiology. 2019;76(6):762–773. doi:10.1007/s00284-018-1510-4

22. Coburn B, Grassl GA, Finlay BB. *Salmonella* , the host and disease: a brief review. Immunology & Cell Biology. 2007;85(2):112–118. doi:10.1038/sj.icb.7100007

23. Questions and Answers | Salmonella | CDC. 2022 Sep 13 [accessed 2023 Jan 15]. https://www.cdc.gov/salmonella/general/index.html

24. Carden S, Okoro C, Dougan G, Monack D. Non-typhoidal Salmonella Typhimurium ST313 isolates that cause bacteremia in humans stimulate less inflammasome activation than ST19 isolates associated with gastroenteritis. Pathogens and Disease. 2015 [accessed 2023 Jan 15];73(4). http://academic.oup.com/femspd/article/doi/10.1093/femspd/ftu023/602694/Nontyphoidal-Salmonella-Typhimurium-ST313-isolates. doi:10.1093/femspd/ftu023

25. Wang X, Biswas S, Paudyal N, Pan H, Li X, Fang W, Yue M. Antibiotic Resistance in Salmonella Typhimurium Isolates Recovered From the Food Chain Through National Antimicrobial Resistance Monitoring System Between 1996 and 2016. Frontiers in Microbiology. 2019;10:985. doi:10.3389/fmicb.2019.00985

26. Fang FC, Chen CY, Guiney DG, Xu Y. Identification of sigma S-regulated genes in Salmonella typhimurium: complementary regulatory interactions between sigma S and cyclic AMP receptor protein. Journal of Bacteriology. 1996;178(17):5112–5120. doi:10.1128/jb.178.17.5112-5120.1996

27. Howells AM, Bullifent HL, Dhaliwal K, Griffin K, García de Castro A, Frith G, Tunnacliffe A, Titball RW. Role of trehalose biosynthesis in environmental survival and virulence of Salmonella enterica serovar typhimurium. Research in Microbiology. 2002;153(5):281–287. doi:10.1016/S0923-2508(02)01321-9

28. McClelland M, Sanderson KE, Spieth J, Clifton SW, Latreille P, Courtney L, Porwollik S, Ali J, Dante M, Du F, et al. Complete genome sequence of Salmonella enterica serovar Typhimurium LT2. Nature. 2001;413(6858):852–856. doi:10.1038/35101614

29. Knuth K, Niesalla H, Hueck CJ, Fuchs TM. Large-scale identification of essential Salmonella genes by trapping lethal insertions: Essential Salmonella genes. Molecular Microbiology. 2004;51(6):1729–1744. doi:10.1046/j.1365-2958.2003.03944.x

30. Shao Y, Lin AH-M. Improvement in the quantification of reducing sugars by miniaturizing the Somogyi-Nelson assay using a microtiter plate. Food Chemistry. 2018;240:898–903. doi:10.1016/j.foodchem.2017.07.083

31. Madeira F, Pearce M, Tivey ARN, Basutkar P, Lee J, Edbali O, Madhusoodanan N, Kolesnikov A, Lopez R. Search and sequence analysis tools services from EMBL-EBI in 2022. Nucleic Acids Research. 2022;50(W1):W276–W279. doi:10.1093/nar/gkac240

32. Robert X, Gouet P. Deciphering key features in protein structures with the new ENDscript server. Nucleic Acids Research. 2014;42(W1):W320–W324. doi:10.1093/nar/gku316

33. Jurrus E, Engel D, Star K, Monson K, Brandi J, Felberg LE, Brookes DH, Wilson L, Chen J, Liles K, et al. Improvements to the APBS biomolecular solvation software suite. Protein Science. 2018;27(1):112–128. doi:10.1002/pro.3280

34. Jumper J, Evans R, Pritzel A, Green T, Figurnov M, Ronneberger O, Tunyasuvunakool K, Bates R, Žídek A, Potapenko A, et al. Highly accurate protein structure prediction with AlphaFold. Nature. 2021;596(7873):583–589. doi:10.1038/s41586-021-03819-2

35. Varadi M, Anyango S, Deshpande M, Nair S, Natassia C, Yordanova G, Yuan D, Stroe O, Wood G, Laydon A, et al. AlphaFold Protein Structure Database: massively expanding the structural coverage of protein-sequence space with high-accuracy models. Nucleic Acids Research. 2022;50(D1):D439–D444. doi:10.1093/nar/gkab1061

36. Su J, Gong H, Lai J, Main A, Lu S. The Potassium Transporter Trk and External Potassium Modulate *Salmonella enterica* Protein Secretion and Virulence. Infection and Immunity. 2009;77(2):667–675. doi:10.1128/IAI.01027-08

APPENDIX

Table A1. Site-Directed Mutagenesis Primers

Name	**Description**	**Sequence (5'→ 3')**
SDM1F	The forward primer used in site-directed mutagenesis to produce StMTSase-M460Y-V464Y. The mutant codons are highlighted.	CAACTCACCGGTCCGCTGTATGCGAAATCGTATGAGGATACGCTTTTCTTTCG
SDM1R	The reverse primer used in site-directed mutagenesis to produce StMTSase-M460Y-V464Y. The mutant codons are highlighted.	CGAAAGAAAAGCGTATCCTCATACGATTTCGCATACAGCGGACCGGTGAGTTG
SDM2F	The forward primer used in site-directed mutagenesis to produce StMTSase-M460Y. The mutant codon is highlighted.	AGCAACTCACCGGTCCGCTGTATGCGAAATCGGTAGAGGATAC
SDM2R	The reverse primer used in site-directed mutagenesis to produce StMTSase-M460Y. The mutant codon is highlighted.	GTATCCTCTACCGATTTCGCATACAGCGGACCGGTGAGTTGCT

Table A2. Bacterial Strains

Strain	**Description**	**Selectable Marker**	**Source**
DH5α	*Escherichia coli* cells used for plasmid production, isolation, and storage	None	Storm Lab
BL21	*Escherichia coli* cells used for protein overexpression and purification	None	Storm Lab

Table A3. Plasmids

Name	**Description**	**Selectable Marker**	**Source**
pMcSGJ3	Plasmid containing wild-type StMTSase in fusion with a polyhistidine tag	Ampicillin	CSGID
pMcSGJ3-M460Y-V464Y	Plasmid containing StMTSase in fusion with a polyhistidine tag and with M460Y and V464Y mutations	Ampicillin	Constructed
pMcSGJ3-M460Y	Plasmid containing StMTSase in fusion with a polyhistidine tag and with an M460Y mutation	Ampicillin	Constructed

Table A4. Sequencing Results

Identity	**Sequencing Results (start and stop codons highlighted green; mutant codons highlighted yellow)**
pMcSGJ3-M460Y-V464Y, Coding Strand	CCTTGAGGTAATTCCCTCTAGAATAATTTTGTTTAACTTTAA GAAGGAGATATACATATGCACCATCATCATCATCATTGAGA ACCTGTACTTCCAATCCAATGCCATGATCCCAACTGCAACG TATCGCCTTCAGTTTCGCAATGGCATGACCTTCGATCGCGCT GCGGCGCTGGTGCCTTACCTTAAAAATCTGGGTATCAGCCA TCTTTATGCCTCACCCATCTTTACCGCCACCAAAGCGTCAAC GCATGGTTATGATGTCACCGATGCGAATGAGATTGAGCCTT CTATTGGCGGGCGCGAAGGATTTGAAAGACTGGTGGCTGAA CTTAAAGCGCAAGGTCTGGGATTGATCATCGATATTGTGCC TAATCACATGGCCAGCTCGCTGGAAAACGCCTGGTGGCGCG ACGTGCTTGAATATGGCAAGGAGAGCCGTTACGCGCGCCAT TTCGATATTGACTGGTCGCGCCGACTGACGCTGCCTTTTTTA GGCGACACGTTTGACGCCGTGCTGGAAAACGGAGAAATTGC GATCAAGCCCGATCCCGCTACGGGTAAACCCGCGTTCGCCT ATTATGATAACTATTATCCGCTTGCGCCGGCGACGTGGCAG GGGCGCGAGGCTGAAATACTGGCGCTTACCGATAAAGCCGC TATTGCTGATTTGCATGAGCGCCAGCCGTGGAAATTAATGT CCTGGCGCGATGCCGCTCGCTCGCTTTCATATCGGCGTTTCT TTGAGGTCACAGGGCTGGTAGGAATGCGGGTGGAAGATAA AACCGTCTTCGACGATACACATCGGCTGATTCTGGAGCTGG TCAGAACGGGGGCGGTTGACGGTTTACGTATCGATCATATC GACGGCCTTGCCGATCCGAAAGCCTATCTTGCGCGTTTACG TCAGGAAGTGGGGCCGGCGTGCTATATCACCGTGGAAAAA ATTCTCGCTAAAGGCGAGCAACTTCCTGATGACTGGCCGGT TTCCGGCACCACAGGCTATGAATTTATCGCCTCGCTGGCGG AGGTGCTGGTTGACGATGAGCAGATAGACAATCTGCGCCAG GCTTACGAGACCGTAAAAGGCGCGCCAGTGGATATGCGGG CGGAATTACGGGCGGCTAAATTGCTGATGGTCGATCGCAAT TTCGAGGGGGAATTTACCCGGCTGCTCGCGCTTGCGCTGTC GATTGCCAGCGAGCTACAGATCGCACAGGAAGAGAGCGTC GTTCGGCAGGCGTTACGCGAGTTATTAATTGCCTTTCCCGTA TATCGCACTTACGGCACGGCAGAAGGGCTACCACCGACCGA TATTTGCCTGTTACACCGTATTGTGGAACGGGTAAAGACGC TTGAAACCCCTCCGCAGCCAGAAGCGCTTACATTTCTGAGC CGTCTTCTTACCGGCGATGTTCCCGCCTCCAGCCAGGAGGA GGCGACACAGTTTCGCGTTCGGTTCCAGCAACTCACCGGTC CGCTGTATGCGAAATCGTATGAGGATACGCTTTTCTTTCGTC AAAACATGGGACTGGCGTTAAATGAAGTCGGCGCCGAGCC CGTCACGCATCACTTCTCCATCGAACGCTTTCACCATGAGAT GAAAACCCGACAGGCGCGACAGCCTGATGCGTTATCCGGTA CGTCGACCCACGATACCAAGCGAGGCGAGGATGCGCGAGC ACGCCTGTATACGCTTACCGAAGCGCCGGAGCAGTGGAGCG AATGCCTTGCCCGCTGGCGGCAGATGAACCAGACCCATGTC

	AAATTTTTGAATGATGGCACTGCGCCAAAATCGGCGGATAC GTGGATGTTATATCAGGCGCTGACCGGCGTCTGGCCCCCGG TGCTACAACCACAGGATGAAACAGGCCTAAACGCGCTGAA AACACGCTTTGAAGCCTTTGTGGAGAAAGCGCTACGCGAAG CGAAGCTGCGTACCGATTGGGTGGACAGTAATGAGGCTTAC GAAACGGCAATGCTTGATTACGCCCGTTATTTACTGGCGCC GGATAATCAGACATTTTTGCAGGATTTTTATCGTTCCTTGCA ACCCTTCATCCGCGCAGGACTGGTTAACAGCCTGACGCAGA CCGTTATCAAATTAACCGCGCCGGGAGTACCTGATATCTAT CAGGGAAGCGAGGCGTTGAATTTTAGTCTTGTCGATCCCGA CAACCGCCGCGAACCGGATTTCGCCACGCTGGCGCAGCAGT TAGACCAACTGACGCCGGGAGTTTTCTCGCGCGAAGAGAGT TGGCTGAACGGGCAGGTGAATCAGTATGTCACCGCCGCATT ACTGCGTCTGCGTCAGCAGAATCATGAGCTCTTCCGTTTTGG CGACTATATACCGCTGCGGGCTGTTGGTCAGCGTGCCGACA AGGTCATCGCTTACGCCAGAGTCAATCATGATGATGCGCTG ATTGTTGTTGCGCCCCGACTGGTGTTCGCCGAATGTGACGG CTTATTGTCACAATCGCATAGCGGTTTCTGGTCAGGAACCG ACATTATTATACCCGGACAGCTTAATCAGCATCGTTATCGC AATGTGCTTACCCAGGAGAGGTTAATGCCTGGTGAACGCCT GTCGTTGGCCTCACACCAGGGCGGCGTACTGGTTTTAATGA GCGACTAACATTGGAAGTGGATAACGGATCCGAATTCGAGC TCCGTCGACAAGCTTGCGGCCGCACTCGAGCACCACCACCA CCACCACTGAGATCCGGCTGCTAACAAAGCCCGAAAGAAGT ANCCGAA
pMcSGJ3-M460Y, Coding Strand	AAACNNTTNAGATCCATCGGGCTGATTCTGGAGCTGGTCAG AACGGGGGCGGTTGACGGTTTACGTATCGATCATATCGACG GCCTTGCCGATCCGAAAGCCTATCTTGCGCGTTTACGTCAG GAAGTGGGGCCGGCGTGCTATATCACCGTGGAAAAAATTCT CGCTAAAGGCGAGCAACTTCCTGATGACTGGCCGGTTTCCG GCACCACAGGCTATGAATTTATCGCCTCGCTGGCGGAGGTG CTGGTTGACGATGAGCAGATAGACAATCTGCGCCAGGCTTA CGAGACCGTAAAAGGCGCGCCAGTGGATATGCGGGCGGAA TTACGGGCGGCTAAATTGCTGATGGTCGATCGCAATTTCGA GGGGGAATTTACCCGGCTGCTCGCGCTTGCGCTGTCGATTG CCAGCGAGCTACAGATCGCACAGGAAGAGAGCGTCGTTCG GCAGGCGTTACGCGAGTTATTAATTGCCTTTCCCGTATATCG CACTTACGGCACGGCAGAAGGGCTACCACCGACCGATATTT GCCTGTTACACCGTATTGTGGAACGGGTAAAGACGCTTGAA ACCCCTCCGCAGCCAGAAGCGCTTACATTTCTGAGCCGTCTT CTTACCGGCGATGTTCCCGCCTCCAGCCAGGAGGAGGCGAC ACAGTTTCGCGTTCGGTTCCAGCAACTCACCGGTCCGCTGTA TGCGAAATCGGTAGAGGATACGCTTTTCTTTCGTCAAAACA TGGGACTGGCGTTAAATGAAGTCGGCGCCGAGCCCGTCACG CATCACTTCTCCATCGAACGCTTTCACCATGAGATGAAAAC CCGACAGGCGCGACAGCCTGATGCGTTATCCGGTACGTCGA

	CCCACGATACCAAGCGAGGCGAGGATGCGCGAGCACGCCT GTATACGCTTACCGAAGCGCCGGAGCAGTGGAGCGAATGCC TTGCCCGCTGGCGGCAGATGAACCAGACCCATGTCAAATTT TTGAATGATGGCACTGCGCCAAAATCGGCGGATACGTGGAT GTTATATCAGGCGCTGACCGGCGTCTGGCCCCCGGTGCTAC AACCACAGGA

Table A5. Media and Reagents

TAE Buffer

Component	**Concentration**
Tris-base	40mM
Glacial acetic acid	0.119%
0.5M Ethylenediaminetetraacetic acid (EDTA) (pH 8.0)	0.21%

Agarose Gel 6x Loading Dye

Component	**Concentration**
Glycerol	50%
Tris (pH 8.0)	10mM
Bromophenol Blue	0.25%

Lysogeny Broth (LB)

Component	**Concentration**
Tryptone	1%
Sodium chloride	170mM
Yeast extract	0.5%

S.O.C. Outgrowth Medium

Component	**Concentration**
Tryptone	2%
Yeast extract	0.5%
NaCl	10mM
KCl	2.5mM
$MgCl_2$	10mM
$MgSO_4$	10mM
Glucose	20mM

Miniprep solution 1

Component	**Concentration**
Glucose	50mM
Ethylenediaminetetraacetic acid (EDTA)	10mM
Tris-HCl (pH 8.0)	25mM

Miniprep solution 2

Component	**Concentration**

Sodium dodecyl sulfate (SDS)	1%
Sodium hydroxide	200mM

Miniprep solution 3

Component	**Concentration**
Potassium acetate (pH 5.5)	3.0M

Binding Buffer

Component	**Concentration**
Monosodium phosphate	50mM
Imidazole	10mM
Sodium chloride	300mM

Wash Buffer

Component	**Concentration**
Monosodium phosphate	50mM
Imidazole	40mM
Sodium chloride	300mM

Elution Buffer

Component	**Concentration**
Monosodium phosphate	50mM
Imidazole	200mM
Sodium chloride	300mM

Dialysis Buffer (pH 7.20)

Component	**Concentration**
3-(*N*-morpholino)propanesulfonic acid (MOPS)	20mM
Sodium chloride	100mM
tris(2-carboxyethyl)phosphine (TCEP)	0.2mM

SDS-PAGE 4x Upper Buffer (pH 6.8)

Component	**Concentration**
Tris-base	25mM
Tris-HCl	480mM
Sodium dodecyl sulfate (SDS)	14mM

SDS-PAGE 8x Lower Buffer (pH 8.8)

Component	**Concentration**
Tris-base	2.45M
Tris-HCl	700mM
Sodium dodecyl sulfate (SDS)	28mM

SDS-PAGE 2x Sample Buffer

Component	**Concentration**

Tris-HCl (pH 6.8)	100mM
Sodium dodecyl sulfate (SDS)	5%
Glycerol	30%
Bromophenol blue	0.01%
β-mercaptoethanol (βME)	10%

SDS-PAGE Running Buffer

Component	**Concentration**
Tris-base	25mM
Glycine	19mM
Sodium dodecyl sulfate (SDS)	3.5mM

Coomassie Brilliant Blue

Component	**Concentration**
Methanol	45%
Acetic acid	10%
Water	45%
Coomassie brilliant blue dye	0.25g/L

Coomassie Destain

Component	**Concentration**
Acetic acid	7.5%
Methanol	7.5%
Water	85%

Copper Reagent A

Component	**Concentration**
Sodium potassium tartrate tetrahydrate	70mM
Sodium carbonate	280mM
Sodium bicarbonate	240mM
Sodium sulfate	1.27M

Copper Reagent B

Component	**Concentration**
Copper (II) sulfate pentahydrate	80mM
Sodium sulfate	1.27M

Working Reagent

Component	**Concentration**
Copper reagent A	80%
Copper reagent B	20%

Color Reagent

Component	**Concentration**
Ammonium molybdate	50.4g/L

Sodium arsenate heptahydrate	20mM
Concentrated sulfuric acid	4.2%

McIlvaine Buffer

Component	**Concentration**
Sodium phosphate dibasic	100mM
Citric acid	50mM

Tris-HCl Buffer

Component	**Concentration**
Tris-base	100mM

Sodium Carbonate Bicarbonate Buffer

Component	**Concentration**
Sodium carbonate anhydrous	100mM
Sodium bicarbonate	100mM
*Appropriate volumes of the sodium carbonate and sodium bicarbonate solutions were mixed to produce the desired pHs	